

Evaluating the galaxy formation histories predicted by a neural network in pure dark matter simulations

Harry George Chittenden,^{1,2*} Jayashree Behera³ and Rita Tojeiro²

¹Centre for Astrophysics and Supercomputing [CAS], Swinburne University of Technology, P.O. Box 218, Hawthorn VIC 3122, Melbourne, Australia

²School of Physics & Astronomy, University of St Andrews, North Haugh, St Andrews KY16 9SS, Scotland, United Kingdom

³Department of Physics, Kansas State University, Cardwell Hall, 116, 1228 N M.L.K. Jr. Dr, Manhattan, KS 66506, United States

Accepted XXX. Received YYY; in original form ZZZ

ABSTRACT

We investigate a series of galaxy properties computed using the merger trees and environmental histories from dark matter only cosmological simulations, using the predictive semi-recurrent neural network outlined in Chittenden & Tojeiro (2023), and using stochastic improvements presented in our companion paper: Behera, Tojeiro & Chittenden (2024). We apply these methods to the dark matter only runs of the IllustrisTNG simulations to understand the effects of baryon removal, and to the gigaparsec-volume pure dark matter simulation Uchuu, to understand the effects of the lower resolution or alternative metrics for halo properties. We find that the machine learning model recovers accurate summary statistics derived from the predicted star formation and stellar metallicity histories, and correspondent spectroscopy and photometry. However, the inaccuracies of the model’s application to dark simulations are substantial for low mass and slowly growing haloes. For these objects, the halo mass accretion rate is exaggerated due to the lack of stellar feedback, yet the formation of the halo can be severely limited by the absence of low mass progenitors in a low resolution simulation. Furthermore, differences in the structure and environment of higher mass haloes results in an overabundance of red, quenched galaxies. These results signify progress towards a machine learning model which builds high fidelity mocks based on a physical interpretation of the galaxy-halo connection, yet they illustrate the need to account for differences in halo properties and the resolution of the simulation.

Key words: galaxies: evolution, galaxies: formation, galaxies: haloes, galaxies: star formation

1 INTRODUCTION

Cosmic hydrodynamical simulations are a valuable tool for modelling the causal relationship between galaxies and haloes across cosmic time; known as the galaxy-halo connection (GHC). Modelling galaxy evolution in its full complexity, however, is a difficult task. Numerous physical processes such as the accretion and cooling of gas are necessary to fuel star formation and synthesise heavy elements (Somerville & Davé 2015; Vogelsberger et al. 2020), which in turn are influenced by the growth of the dark matter halo and its interactions with the surrounding cosmological structures (Wechsler & Tinker 2018). Capturing the complete GHC requires details of large scale structure evolution on megaparsec scales to compute massive galaxies and clusters, and the physics internal to the galaxy to compute summary statistics such as mass-metallicity relations.

In Chittenden & Tojeiro (2023), hereafter CT23, we designed a semi-recurrent neural network capable of reproducing the GHC in the Illustris: The Next Generation (TNG) simulations (Nelson et al. 2017, 2019a; Pillepich et al. 2017a; Springel et al. 2017; Marinacci et al. 2018; Naiman et al. 2018), in which we predict the star formation history (SFH) and metallicity history (ZH) of central and satellite galaxies, from which we recover physical relations such as the stellar-halo mass relation (SHMR) and mass-metallicity relation

(MZR), reproduce observational statistics such as colour bimodality, and show the growth and internal properties of the halo to influence the predicted SFH and stellar mass, while environmental properties influence the ZH and stellar metallicity.

Machine learning models which can emulate galaxy properties from their dark matter component alone can be used to make predictions in cosmic N-body simulations, where the absence of galaxies allows for such simulations to be computed with much greater size and resolution than their hydrodynamical counterparts. Many studies would benefit from a simulation containing galaxy evolution on these scales (Habouzit et al. 2022; Tanaka et al. 2023; Kurinchi-Vendhan et al. 2024), however the limited computational resources required for such simulations make computing such a hydrodynamical suite highly impractical.

In this paper, we explicitly evaluate the performance of the trained galaxy evolution model on N-body simulations. Predictions are expected to be somewhat different in dark simulations due to the lack of baryonic effects on the halo mass function (Castro et al. 2020; Anbajagane et al. 2021; Hagger et al. 2021; Riggs et al. 2022), and due to differences in mass and spatial resolution, and alternative definitions or calculations of key halo and environmental properties. We compare predictions in the hydrodynamical TNG simulations, discussed at length in CT23, with the equivalent dark simulations in the TNG suite (hereafter TNG-Dark), and the Uchuu dark matter simulation (Ishiyama et al. 2021).

* E-mail: hchittenden@swin.edu.au

Uchuu is a high fidelity N-body simulation which assumes the same [Planck Collaboration \(2016\)](#) cosmological parameters as all TNG simulations, therefore there are little to no effects to consider regarding mean matter density or Hubble expansion. By comparing predictions in TNG-Hydro with TNG-Dark, we isolate the effect that baryons have on the predicting power of the neural network. By comparing TNG-Dark with Uchuu, we show the effect of Uchuu's lower resolution and alternative definitions of halo properties. The predictions made in Uchuu are therefore the simplest results to be expected for a high fidelity galaxy catalogue produced using our model.

Further to this endeavour, we apply a stochastic modification to the N-body simulation predictions, whose methods and improvements to our TNG-Hydro-based galaxy-halo statistics are outlined in [Behera, Tojeiro & Chittenden \(2024\)](#), hereafter *BTC24*. It is shown in [CT23](#) that the machine learning model alone is inadequate for predicting star formation events on short timescales, in spite of the success of predicting the general evolution of galaxies across all times. These "stochastic" features are well recovered by this correction, and the results of *BTC24* illustrate that certain missing properties of our fiducial galaxy-halo statistics can be attributed to the physics of variable star formation. We apply this modification to the TNG-Dark and Uchuu data to assess the plausibility of reproducing this variability in N-body mocks.

In this paper, we investigate the quality of predictions between our original results and the predictions in TNG-Dark and Uchuu, explain systematic differences between the results in each of these simulation suites and discuss the suitability of our model for reproducing galaxies in a pure dark matter simulation. In Section 2 we discuss the definitions of the dark matter data in each of the simulations, and our methods of acquiring the necessary input data. We compare properties of the input data in Section 3, baryonic predictions in Section 4 and observational results in Section 5, elucidating their disparities each time, and exhibiting the improvements made by the stochastic amendment introduced in *BTC24*. We evaluate the successes and failures of the model, the stochastic correction, and their proficiency for modelling the GHC on gigaparsec scales in Section 6, and summarise our findings in Section 7.

2 DATA ACQUISITION

In this section, we describe how the data from the pure dark matter simulations are processed for use in our neural network, and discuss the effects of fundamental differences between these simulations on the quality of our data.

Full details regarding data processing are given in [CT23](#), however the data processing procedure can be summarised as follows:

- Calculate mass accretion histories by finite differencing the (sub)halo mass along the main progenitor branch (MPB).
- Interpolate the MPB over the time domain of every third snapshot in TNG, down to and including $z = 0$.
- For each of these snapshots, calculate overdensities and skews¹ using the Grid Search In Python (GriSPy) package ([Chalela et al. 2021](#)).
- Compute the proxy for circular velocity history: the square root of the ratio of (sub)halo mass (M_{\odot}) to half-mass radius (Mpc).

¹ A measure of the mass-weighted radial distribution of subhaloes exterior to the target subhalo, tracing subhalo interaction history, as discussed in [CT23](#).

- For satellites, compute infall parameters, e.g. scaled infall time, infall velocity, based on and including the scaled accretion time from [Shi et al. \(2020\)](#); from the MPBs of the satellite and its host halo. If the simulation contains baryonic data, discard any samples where the stellar mass of the host halo is greater than 10% of the halo mass.

- For centrals, acquire the $z = 0$ cosmic web properties calculated using the Discrete Persistent Structure Extractor (DisPerSE) code ([Sousbie 2011](#)). The TNG-Hydro results are publicly available².

- Calculate the specific mass accretion gradients shown in [Montero-Dorta et al. \(2021\)](#). Fit a Gaussian function to the distribution of gradient values, and discard any samples whose gradient is over 5σ from the mean of the best fit Gaussian.

- Apply a Gaussian quantile transformation (GQT) to the input data where necessary, using time-independent transformations for most temporal variables. Apply this transformed data to the network.

This gives a list of quantities used in the neural network model, summarised in table 1. As in [CT23](#), we use the integrated stellar masses and mass-weighted metallicities derived from predicted SFHs and ZHs to produce summary statistics such as the SHMR and MZR, and use the Flexible Stellar Population Synthesis (FSPS) code ([Conroy et al. 2009](#); [Conroy & Gunn 2010](#)) to calculate SEDs and other observables from these network output quantities.

2.1 TNG-Dark

Table 2 shows the key differences between the simulations used in this work. The TNG-Dark simulations are of similar resolution to their hydrodynamical counterparts, and therefore resolution effects will be small if at all applicable. The time domains of their snapshots are also equivalent. The crucial difference between the two results is therefore due to the absence of baryonic effects on the haloes in the TNG-Dark simulations.

In order to interpret the differences between the dark and hydrodynamical TNG simulations, we select samples in the dark simulation by cross-matching SubLink trees with our original, hydrodynamical dataset ([Nelson et al. 2015](#); [Rodriguez-Gomez et al. 2015](#)), and samples with no cross-matched result in TNG-Dark are discarded. In [fig. 1](#) we show that for central haloes this has little effect on the $z = 0$ halo mass distribution of our data, yet for satellite objects the number of samples begins to decline sharply below $\sim 4 \times 10^{10} M_{\odot}$.

Generally, objects in one simulation are not accurately matched to the other for two reasons. Firstly, objects in proximity to much larger haloes may pass within the virial radius of the larger halo in one of the two simulations, allowing for central haloes to be matched to satellites, and vice versa. Similarly, and particularly so for low mass objects, the SubFind algorithm may combine two distinct subhaloes into a single object, such that one low mass subhalo will cease to exist in the lower resolution simulation (TNG-Dark). These effects eliminate $\sim 39\%$ of our satellite subhaloes compared with $\sim 1\%$ of our central haloes.

Most TNG-Dark variables were computed in the same manner as the data from hydrodynamical simulations. The exception is the $z = 0$ DisPerSE cosmic web distances, which, due to the geometric correspondence of the hydrodynamical and dark simulations, are identical to their cross-matched counterparts. We therefore assign the cosmic web properties of TNG-Hydro samples to their cross-matched equivalents in TNG-Dark, in lieu of publicly accessible data for the latter.

² https://github.com/Chris-Duckworth/disperse_TNG/

| Network Data | | | | |
|-----------------------------|--|--|-------------------------------|----------------------|
| | Quantity | Notation | Units | Network |
| Temporal Features | Halo Mass Accretion Rate | \dot{M}_h | M_\odot/Gyr | Both |
| | Subhalo Mass Accretion Rate | \dot{m}_h | M_\odot/Gyr | Satellite |
| | 1Mpc Overdensity | δ_1 | | Both |
| | 3Mpc Overdensity | δ_3 | | Central |
| | 5Mpc Overdensity | δ_5 | | Central |
| | Circular Velocity (proxy) | \bar{v}_{vir} | $\sqrt{(M_\odot/\text{Mpc})}$ | Both |
| | Dark Matter Half-Mass Radius | $R_{\frac{1}{2}}$ | Mpc | Both |
| | 1Mpc Radial Skew | μ_3 | | Satellite |
| | 3Mpc Radial Skew | μ_3 | | Central |
| | Distance To Closest Subhalo | d_{μ_3} | Mpc | Both |
| Non-Temporal Features | Specific Halo Mass Accretion Gradient | β (c) β_{halo} (s) | $\log \text{Gyr}^{-2}$ | Both |
| | Specific Subhalo Mass Accretion Gradient | β_{sub} | $\log \text{Gyr}^{-2}$ | Satellite |
| | Scaled Infall Time | a_{infall} | | Satellite |
| | Scaled Formation Time | a_{max} | | Satellite |
| | Infall Mass Ratio | μ | | Satellite |
| | Infall Velocity | v_{rel} | km/s | Satellite |
| | $z = 0$ Cosmic Web Distances | d_{CW} | kpc | Central |
| | Starting Time | t_{start} | Gyr | Both |
| | $z = 0$ Halo Mass | M_h | M_\odot | Both |
| | Maximum Absolute Halo Accretion Rate | $ \dot{M}_h $ | M_\odot/Gyr | Both |
| | $z = 0$ Subhalo Mass | m_h | M_\odot | Satellite |
| | Maximum Absolute Subhalo Accretion Rate | $ \dot{m}_h $ | M_\odot/Gyr | Satellite |
| | Targets | Star Formation History | \mathcal{S} | M_\odot/Gyr |
| Metallicity History | | \mathcal{Z} | Z_\odot | Both |
| $z = 0$ Stellar Metallicity | | Z | Z_\odot | Both |
| $z = 0$ Stellar Mass | | M_s | M_\odot | Both |
| Mass Weighted Age | | MWA | Gyr | Both |

Table 1. Simplification of Table 1 in CT23, summarising the quantities used in both neural networks, according to their input and output layers and their arrangement in the network. Additional columns show the variables' units, and the central and/or satellite networks which use them.

2.2 Uchuu

2.2.1 Merger Forests

Uchuu merger trees are grouped into 2,000 "Forests": ensembles of merger trees which contain all haloes which have interacted with any given member of the forest, and occupy a volume of space separate from all other forests. Each forest can therefore be treated independently of another, as the Consistent-Trees code (Behroozi et al. 2012b) used to define merger trees in Uchuu is run independently in groups which occupy a fixed volume, which are then concatenated if they interact or pass within $25 \text{ Mpc}/h$ of each other (Ishiyama et al. 2021).

In this work we use forest 1411, the largest Uchuu forest, and acquire similar samples to the TNG dataset by drawing from the TNG-Dark halo mass distribution and sampling the Uchuu forest at $z = 0$ accordingly, which is shown by fig. 1. This results in approximately 30,000 central and satellite haloes each.

As the chosen Uchuu forest has a geometric mean side length of approximately 234 Mpc, it is of similar volume to the TNG simula-

tions, and thus for high mass objects, sampling the (sub)halo mass distributions effectively approximates the (sub)halo mass functions of Uchuu. At lower masses, sampling Uchuu according to the TNG-Dark distribution ensures that the properties in different mass ranges can be compared without sample size bias. While this selection constitutes our test data for the neural network, environmental quantities are computed using the complete Uchuu forest, and are considered unbiased due to the TNG and Uchuu simulations having the same cosmic matter density parameters.

We use the YTree Python package to extract the main progenitor branches from the Uchuu forest. The quantities we obtain directly from the forest include halo mass, half mass radius, positions and peculiar velocities. Cosmic web distances are obtained by applying DisPerSE to the forest, which being a self-consistent subset of Uchuu means that the algorithm does not need to be applied to the full Uchuu simulation. All other quantities, such as overdensities, are calculated using the same methods as in CT23.

2.2.2 Alternative Definitions

Unlike TNG, SubLink merger trees do not exist in Uchuu, and haloes and their substructures are defined using the Rockstar code (Behroozi et al. 2012a). There exists a flag in each Uchuu merger tree which indicates the ID of the halo which hosts the target halo. A "first order" satellite halo is one whose host is a central "zeroth order" halo, a "second order" halo is hosted by a first order halo, and so on. We therefore treat first order haloes as satellite haloes, and zeroth order haloes as central haloes.

In TNG, halo and subhalo masses are taken as the sum of all masses of dark matter particles bound to the group by the SubLink algorithm. This field does not exist in the Uchuu merger trees, however a number of definitions of mass exist. We find that the closest match to this field which exists in both suites is M_{200c} : the total mass enclosed within an overdense region equal to 200 times the critical mass density of the universe. These mass accretion histories show similar behaviour in TNG-Dark and Uchuu, and produce a similar overall mass distribution, and consequently the predictions of the neural network are similar when trained using M_{200c} and with the SubLink mass. This is our choice of field representing halo masses in Uchuu. Halo mass dependent calculations such as overdensities are also calculated using this quantity.

2.2.3 Resolution Differences

Table 2 shows that the mass resolution of Uchuu is an approximate order of magnitude weaker than the TNG300 simulations. This results in very poor resolution of low mass haloes in Uchuu, and the absence of low mass first order satellite haloes, following quality cuts such as the omission of samples whose specific mass accretion gradients differ from the mean by more than 5σ , serves to limit the number of satellites below a subhalo mass of $\sim 2 \times 10^{11} M_\odot$, which we show in fig. 1. We are left with a modest sample of low mass satellite haloes but a clearly different distribution of subhalo masses below $\sim 2 \times 10^{11} M_\odot$.

Another important detail is the difference in time resolution of the Uchuu snapshots compared with TNG. Uchuu has half as many snapshots as TNG, as shown in table 2, however the temporal separation of snapshots is smaller than TNG for $2 \lesssim z \lesssim 4$ and larger otherwise. All temporal properties, regardless of their simulation, are linearly interpolated over the same 33 snapshots in TNG, yet the sparse nature of these snapshots means that information on short timescales may be lost.

| Simulation Properties | | | | |
|-----------------------|---------------|------------------------|---------------------------------|-------------------|
| Suite | Simulation | L_{box} (Mpc) | m_{DM} (M_{\odot}) | N_{snap} |
| TNG - Hydro | TNG100-1 | 110.7174 | 7.5×10^6 | 100 |
| | TNG300-1 | 302.6277 | 5.9×10^7 | 100 |
| TNG - Dark | TNG100-1-Dark | 110.7174 | 8.9×10^6 | 100 |
| | TNG300-1-Dark | 302.6277 | 7.0×10^7 | 100 |
| Uchuu | Uchuu | 2952.4653 | 4.8×10^8 | 50 |

Table 2. Properties of the simulations used in this work, relating to their volume and resolution. L_{box} indicates the side length of the comoving cubic volume of the simulation, m_{DM} represents the mass of a single dark matter particle, i.e. the smallest possible mass in the simulation, and N_{snap} represents the total number of time snapshots in the simulation. Simulations are grouped in this table according to the suite of simulations (e.g. TNG-Dark) from which they originate. For all of these simulations, mass resolution is decreased as the volume of the simulation and number of particles are increased.

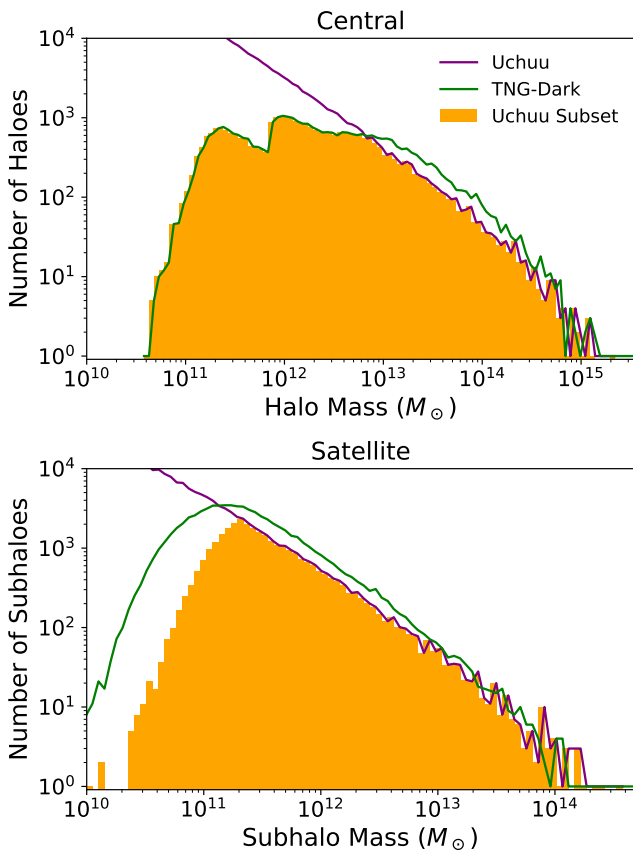


Figure 1. Distributions of central halo and satellite subhalo masses in the complete Uchuu forest (purple) and our cross-matched TNG-Dark sample (green). Sampling the former distribution according to the latter, we obtain the distribution of Uchuu haloes used in this work (orange). The distribution of central haloes is similar to the TNG-Dark data, however the lack of well-resolved satellite subhaloes at low mass serves to bias the sample distribution of satellite subhaloes in our Uchuu dataset.

3 HALO PROPERTIES

For each simulation used in this study, we apply the same algorithm to acquire the input data, however there exist key differences between the definitions of these properties, depending on the model in question; and differences in their statistics due to the removal of baryons or the resolution of the data. In this section, we discuss the

similarities and differences between key input properties of the neural network in each simulation, and how this may influence the predictions of the neural networks.

We compare properties for central and satellite haloes in bins of different mass and accretion history to investigate these differences in separate evolutionary regimes. For centrals, we characterise haloes of different accretion histories according to the specific mass accretion gradient, denoted β , which [Montero-Dorta et al. \(2021\)](#) show to be clearly correlated with gas fraction, quenching timescale and assembly bias in TNG300. We use this quantity for quality cuts in both central and satellite datasets, however it is not so useful for modelling satellite subhalo histories due to the distinct nature of the modes of accretion in their central and satellite phases. For satellites, we use the scaled accretion time a_{max} , which, like β , is derived explicitly from the subhalo mass accretion history, and is shown by [Shi et al. \(2020\)](#) to have similar connections with satellite galaxy properties.

In the following figures which compare haloes of different histories, subplots are arranged such that each column is a quintile of (sub)halo mass, with higher mass bins towards the right; while each row is a quartile of accretion gradient, with the steepest accretion histories on the top row. For satellites, higher a_{max} values are placed on the top row, such that in both cases, haloes with the earliest half-mass formation times are placed on the top row. These percentiles are taken from the TNG-Hydro data. This convention is adopted for all figures of this format, such that in each case the earliest-forming, gas-poor halos or subhalos appear on the top row. For simplicity, we show only odd-numbered mass quintiles, and only the first and fourth quartiles of mass accretion gradient.

3.1 Mass Accretion History

Figures 2 and 3 show the median and 15th – 85th percentile ranges of mass accretion histories in bins of final (sub)halo mass and mass accretion gradient. In most bins, these mass accretion histories are very similar. The differences between simulations arise in low mass and shallow gradient cases, where the amplitude of Uchuu mass accretion histories are reduced, and in the low mass regime is increased for TNG-Dark haloes at early times.

The enhancement of mass for early, low mass haloes is likely due to the absence of baryonic driven outflows, which will have a substantial effect on haloes of a high gas fraction. The weaker accretion rates in the Uchuu simulation, however, are a result of the lower mass resolution of the simulation. In shallow gradient bins, there is a clear flat profile to Uchuu accretion histories, being somewhat reminiscent of TNG samples which were discarded by our quality cuts.

With Uchuu being of lower mass resolution than any of the TNG simulations, the resolution of low mass haloes will be poor. In the lowest mass quintile, galaxy evolution may be poorly predicted from the start of the galaxy’s evolution due to the sensitivity of the star formation algorithm in TNG to the number of dark matter particles ([Pillepich et al. 2017b](#)). Haloes with shallower accretion gradients generally form at later times ([Montero-Dorta et al. 2021](#)), as is the case for our Uchuu data, and therefore those in any given mass bin will be of lower mass at any nonzero redshift. They are therefore subject to a similar resolution effect. For satellites with shallow accretion, there is a noticeable decline in the median accretion rate compared with TNG, probably due to the absence of low mass objects being accreted onto the halo.

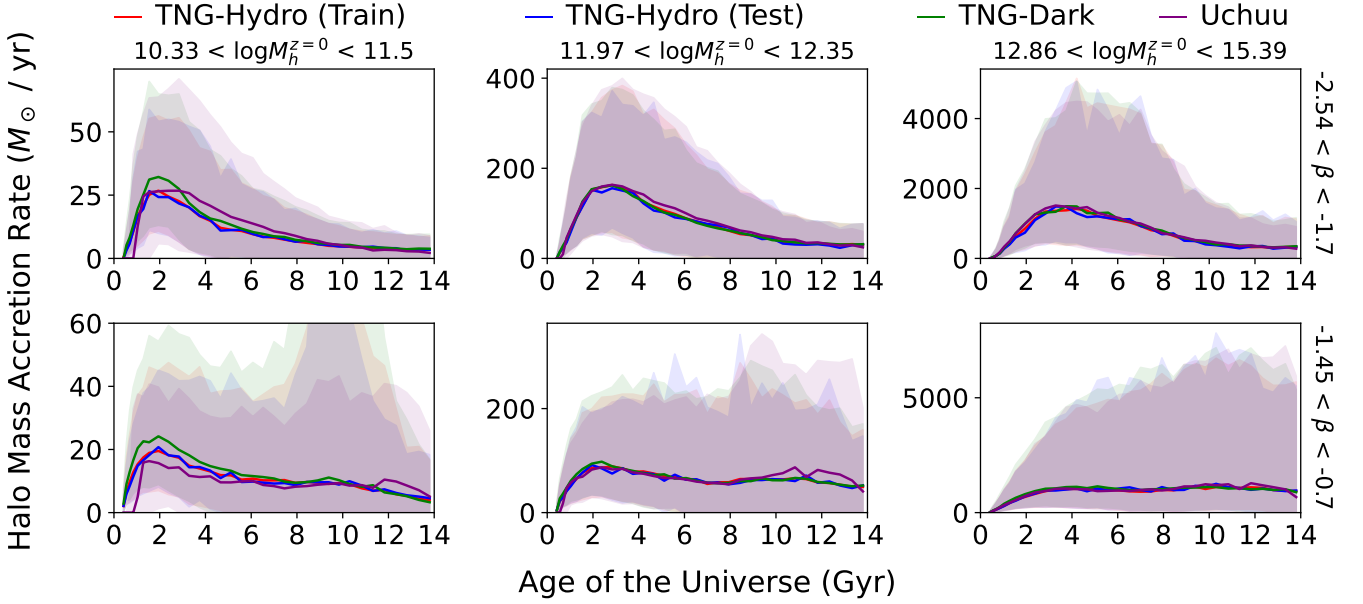


Figure 2. Mass accretion histories of central haloes in bins of halo mass, increasing along the horizontal axis, and specific mass accretion gradient, decreasing in steepness down the vertical axis. Solid lines show the median mass accretion history per bin, while shaded regions show the 15th and 85th percentiles. Mass accretion histories are shown for the training (red) and testing (blue) datasets of the TNG-Hydro simulations, alongside TNG-Dark (green) and Uchuu (purple).

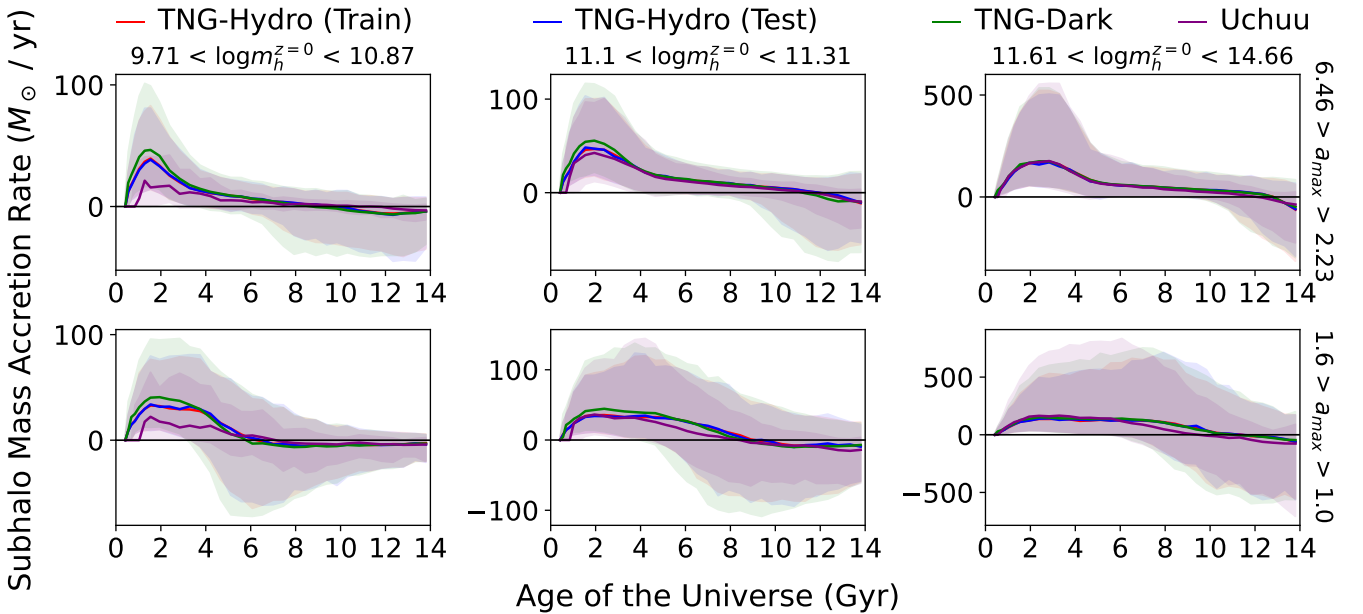


Figure 3. Mass accretion histories of satellite subhaloes, binned in the same manner as in fig. 2, using satellite subhalo mass in place of central halo mass, and scaled accretion time in place of specific mass accretion gradient. One key difference in the properties of these accretion histories is their approach towards zero or negative accretion, which rarely happens for central haloes. Subplots show the different times at which subhalo growth stops in different growth regimes.

3.2 Half-Mass Radius

The quantity which differs most starkly in the Uchuu data, however, is the halo half-mass radius, shown for central and satellite haloes in figs. 4 and 5 respectively. There is a clear deviation in the size evolution of haloes in Uchuu compared with TNG in low mass and shallow gradient bins. However, they are also subtly but noticeably larger in most other bins and at most times.

In TNG-Dark, the half-mass radii of central haloes are subtly smaller in high mass bins than in the other simulations. This may be explained by the results of Haggar et al. (2021) and Riggs et al.

(2022), who show that the number density of haloes which are gravitationally bound to a galaxy group or cluster is underpredicted in dark simulations with respect to their hydrodynamical counterparts, within two virial radii of the cluster or galaxy group. This is caused not only by the high density of baryons in the large object's centre but the effect this has on its own density profile.

Chua et al. (2019, 2022) show that the radial profiles and asymmetries of haloes in TNG, and in the original Illustris simulation, are affected significantly by baryons. According to our data, however, this does not affect the size history in TNG-Dark when compared

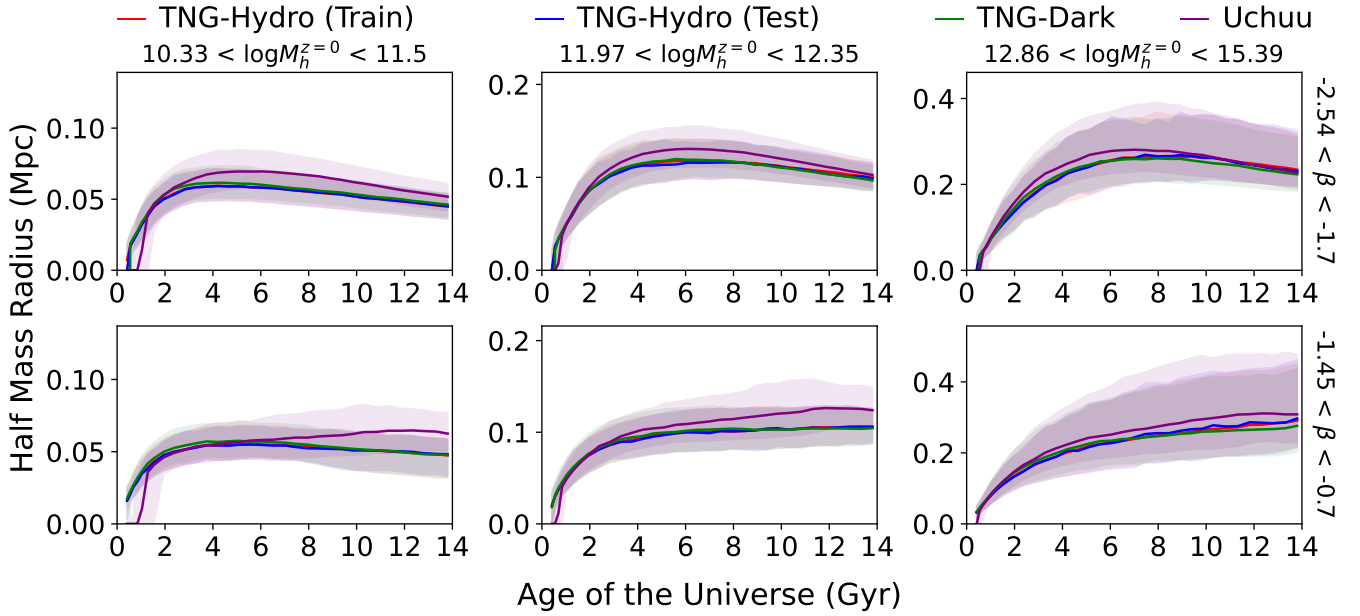


Figure 4. Growth of the half-mass radius of central haloes over time, shown in the same tabular format as fig. 2, with the same bins of halo mass and accretion gradient.

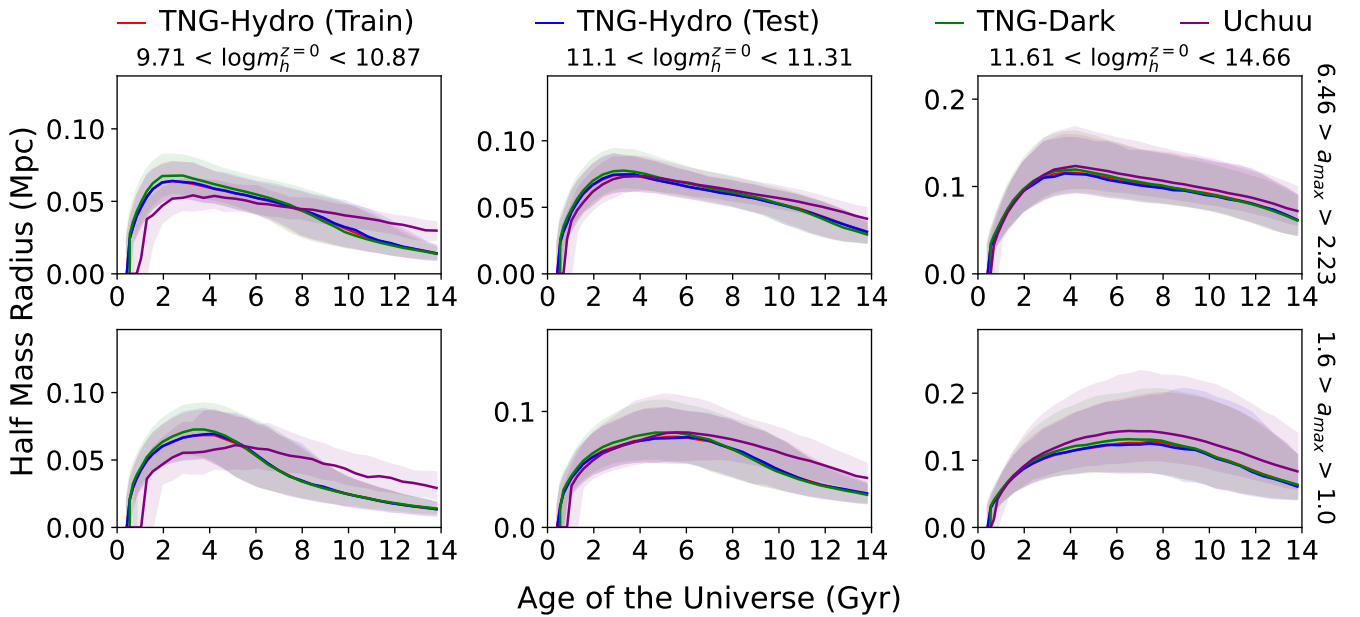


Figure 5. Growth of the half-mass radius of satellite subhaloes over time, shown in the same tabular format as fig. 3, with the same bins of halo mass and scaled accretion time.

with the full physics simulation. In CT23 we thoroughly compared quantities in hydrodynamical and dark TNG simulations at all times to ensure that they could be used in a dark matter simulation. In Uchuu, however, the half-mass radius is defined in terms of virial mass, unlike the SubFind result in TNG.

The SubFind algorithm used in TNG defines the boundaries of a subhalo according to a contour of constant density meeting a saddle point in the local density field (Springel et al. 2001), and the half-mass radius is defined as the radius which encloses half of the mass enclosed by this boundary. In Uchuu, a spherical region whose radius encloses the virial mass is assumed (Ishiyama et al. 2021), and therefore the calculation of half-mass radius is dependent on the

halo density profile. The Rockstar halo finder (Behroozi et al. 2012a) used in Uchuu calculates this profile from the cumulative binding energies of halo particles, and therefore is sensitive to the NFW profile (Navarro et al. 1996) concentration parameter.

Zhao et al. (2009) show that, in N-body simulations, the increase of the NFW concentration parameter over time is scaled by the time of formation of 4% of the final halo mass; while Prada et al. (2012) show that halo concentration is additionally sensitive to fluctuations in the linear density field on the scale of the halo’s mass. These are both quantities which will depend on the resolution of the simulation, however this effect on the growth of halo concentration is most likely reflected in the more extended mass distributions at

late times, as well as the smaller radii of low mass haloes at early times. Ishiyama et al. (2021) also show that in the smaller, higher resolution Shin-Uchuu simulation, while the halo mass functions do not differ significantly between the two Uchuu models, the mass-concentration relation does grow differently between the two simulations, illustrating that this difference in structure is in fact a resolution effect. Morphological halo quantities such as virial velocity and axis ratios are additionally dependent on the gravitational softening scale, which, being larger in Uchuu than in TNG, would result in a flatter $M_h - v_{\max}$ relation at low mass, and thus a similarly distorted mass-concentration relation (Mansfield & Avestruz 2021).

For both central and satellite haloes, it is the youngest, smallest haloes which are most affected by the difference in halo concentration owing to Uchuu’s lower resolution. In each case these haloes are growing from low mass progenitors and thus more likely to suffer from delayed growth in the Uchuu data. Furthermore, Hoffmann et al. (2014) argue that the subhalo finder algorithm makes little difference to the inferred halo shape, provided that the subhalo is comprised of adequately many particles, which low mass, low resolution haloes do not possess. We therefore stress that the delayed growth of the half-mass radius is a resolution effect and not dependent on the algorithm which defines the halo. Yet on the other hand, Onions et al. (2012) argue that Rockstar is superior to most algorithms in identifying halo substructures in dense halo centres, which can affect the half-mass radius value. The fact that some graphics in figs. 4 and 5 show a larger range of radii in Uchuu for all times, suggests that this is also a relevant factor.

3.3 Circular Velocity

The proxy for the virial circular velocity used in our model depends on the above two quantities. It was defined specifically due to extreme differences between the maximum orbital velocities in TNG-Hydro and TNG-Dark, particularly at early times.

Due to the discrepancies we have shown for these quantities in the Uchuu data, the median values for this proxy are slightly too small, but the shape of this median curve remains congruous to its TNG counterparts. In low mass bins, however, this proxy is overestimated in TNG-Dark; most likely as a result of excess mass accretion. This also happens to high mass centrals, however to a smaller extent and owing instead to smaller half-mass radii.

3.4 Cosmic Environment

In CT23 we characterised the environmental histories of central and satellite haloes using subhalo overdensities at each TNG snapshot, and devised a radial skewness quantity which characterised the interaction histories of these haloes. While the mass and structure quantities discussed thus far were deemed important to predicting the star formation histories of the haloes’ galaxies, these environmental properties were shown to predict their chemical enrichment.

As previously discussed, the definitions of halo substructure differ in the Uchuu catalogue, using Rockstar haloes in the place of subhaloes, and thus the overdensity and skew calculations are based on halo tracers. Overdensities in Uchuu are larger than those in TNG-Dark, which can be seen in fig. 6. In a lower resolution simulation, the calculation of environmental quantities is more sensitive to edge effects of the calculation volume, and the radially symmetric definition of a halo in Uchuu can affect the centre of mass of a given object, which may both be contributing factors to the differences in overdensity. Skews, on the contrary, are not noticeably affected by

the resolution difference. As this is a mass-weighted quantity and thus independent of any scaling, it is likely that the difference in overdensities is a result of the mass content of the relevant density tracers.

4 GALAXY PREDICTIONS

Having outlined the causes of differences between haloes and environments in each simulation, we explain in this section how the implementation of these distinct variables into the neural network changes important results. We discuss the effects that the simulation differences have on the direct predictions and derived halo-galaxy relations, providing a physical explanation into differences in the results.

4.1 Star Formation History

Figures 7 and 8 show the median and 15th – 85th percentile ranges of predicted star formation histories in bins of final (sub)halo mass and mass accretion gradient, including the modified star formation histories in the N-body simulations. Each of these figures show that galaxies in high mass and fast accretion bins are typically well matched, but in low mass bins the differences are stark. Star formation rates in TNG-Dark are over-predicted, while in Uchuu they are underpredicted.

From fig. 8 it may appear that the majority of Uchuu galaxies are severely underpredicted in their stellar mass. This is misleading due to the absence of low mass haloes, discussed in section 2.2.3. The two lowest mass quintiles of TNG haloes contain ~ 12% of satellite galaxies in Uchuu. However, these star formation histories are nonetheless severely underpredicted. Their halo histories have already shown that these objects accumulate their mass later and more slowly than their TNG counterparts. This can be seen clearly for satellites in figs. 3 and 5.

In table 3 we show Spearman correlation coefficients between halo and galaxy properties in a narrow, low mass bin for central and satellite objects in Uchuu. Within individual bins at low mass, the final stellar mass is correlated strongly with the proxy for circular velocity, which in the Uchuu data is subtly smaller than its TNG equivalents. Weaker correlations exist with stellar mass and half-mass radius and overdensity, which are also somewhat different in Uchuu.

However, particularly for low mass satellites in fig. 8, underpredicted star formation histories are clearly correlated with similarly undermined mass accretion histories in fig. 3, which will have had a causal effect on their galaxy growth. Mass accretion at early times is particularly important for the acquisition of star-forming gas, which would explain the lack of subsequent star formation in these predictions. In the TNG simulations, low-mass haloes are particularly gas-rich (Davies et al. 2019) and so the star formation at early times is likely to be sensitive to the lack of accumulation of low mass progenitors.

Comparing the network’s performance on TNG-Dark with TNG-Hydro predictions, we see that these star formation histories are enhanced rather than suppressed, which correlates with similarly excessive mass accretion rates. Sorini et al. (2022) show that gas accretion and stellar feedback processes have their greatest influence on the size and shape of haloes and large scale structure at higher redshifts, and that stellar feedback is the principal cause of suppression of the star formation of low mass objects. The lack of stellar

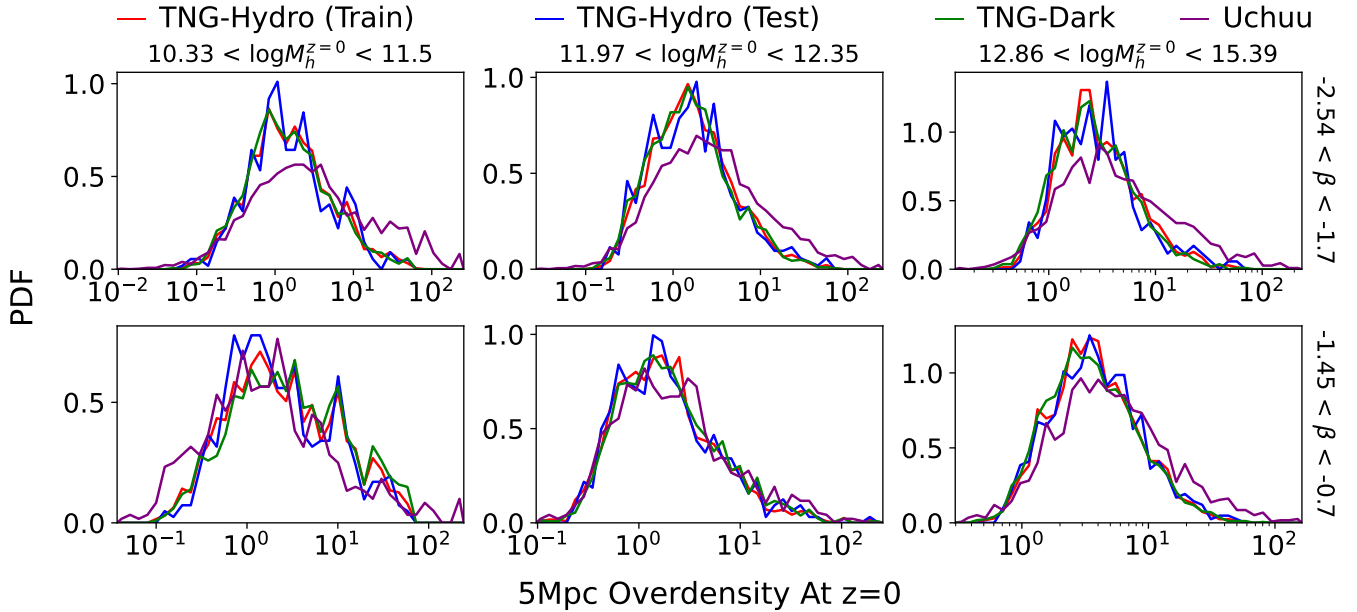


Figure 6. PDFs of the dark matter overdensities enclosed in a 5Mpc spherical region surrounding zero-redshift haloes in the four simulation datasets. These histograms show similar distributions of overdensity for a given mass and accretion history, except for typically larger densities in the Uchuu simulation.

| Input Variable | Stellar Mass | | Metallicity | |
|-------------------|--------------|-----------|-------------|-----------|
| | Central | Satellite | Central | Satellite |
| Circular Velocity | 0.783 | 0.637 | 0.693 | 0.361 |
| Half-Mass Radius | -0.566 | -0.573 | -0.602 | -0.314 |
| Overdensity | 0.176 | 0.298 | 0.174 | 0.142 |

Table 3. Spearman correlation coefficients of multiple halo properties with stellar mass and metallicity, in narrow, low halo mass bins. All quantities shown here are considered at $z = 0$ in the Uchuu simulation. We evaluate these within halo mass ranges of $11.77 < \log_{10} M_h^{z=0} < 11.97$ for centrals, and $10.9 < \log_{10} m_h^{z=0} < 11.1$ for satellites.

feedback in dark simulations will have limited the effects which result in halo mass loss, which are particularly prominent effects for low mass objects. The excess mass accretion in TNG-Dark will have resulted in excess star formation being predicted.

The stochastic modification to our star formation and metallicity histories, explained in detail in [BTC24](#), introduces fluctuations to individual galaxies by drawing random phases from high frequency modes, which are scaled in amplitude according to a predicted Fourier Transform of the sample’s SFH and ZH. By training the neural network introduced in [CT23](#) to predict the Fourier amplitude of each SFH and ZH, while changing none of the input variables or aspects of the network’s design, we predict Fourier amplitudes which resemble those of the original TNG data; unlike the fiducial predictions of the original network, which lose much of this information at high frequencies. A comparison of the Fourier Transforms derived from central star formation histories in an intermediate mass bin is shown in [fig. 9](#).

With the stochastic modification, the additional fluctuations in the star formation histories have recovered enough information that the median and variance of the predictions in both N-body simulations are improved, with the dataset more akin to the target TNG data. However, the correction is less effective for low mass centrals and satellites, and does not resolve the severe offsets seen in Uchuu galaxies.

As star formation histories are poorly predicted for under-resolved Uchuu galaxies, so are their Fourier Transforms, making mass resolution crucial to the stochastic modification as much as the machine learning model itself. We illustrate this in [fig. 9](#), comparing the predicted Fourier amplitudes of each simulation with the desired result from the raw TNG data. For this bin in β and M_h , we can see that the Uchuu Fourier amplitudes are reduced across all frequencies. With the stochastic method sampling high frequency modes with suppressed amplitudes, the same variable star formation history will be lacking in under-resolved Uchuu data, regardless of the efficacy of the stochastic method.

In [BTC24](#), several post-processing filters were applied to mitigate unphysical results in the modified data. For Uchuu and TNG-Dark, an additional threshold is necessary due to unphysical distortions arising from less accurate predictions of the Fourier Transform amplitudes. To address this, we impose a threshold that limits the relative difference between the corrections and the predictions to less than a factor of 1.5, which is typical of the modified TNG-Hydro data. Any larger deviations are replaced by the fiducial predictions to avoid further distortions.

For the TNG-Dark data in this mass/gradient range, the Fourier Transforms resemble the TNG-Hydro predictions, suggesting that the same stochastic data as in [BTC24](#) may appear in TNG-Dark, yet as discussed below, the modifications in TNG-Dark are also subject to certain resolution effects.

Numerically integrating the SFHs of each simulation result in self-consistent and accurate SHMRs, shown in [fig. 10](#). Between predictions in the TNG-Hydro and TNG-Dark simulations, there is little noticeable difference between the relations, other than slightly reduced scatter in the dark predictions. For Uchuu, the difference in stellar and halo mass distributions is apparent, and this is most profoundly so at low masses. From intermediate to high masses, there is a slight underprediction of mass and scatter, but the Uchuu SHMR remains very well matched to the predictions in TNG-Hydro and TNG-Dark.

In both the central and satellite SHMRs, particularly at intermediate masses, the stochastic modification makes subtle improvements

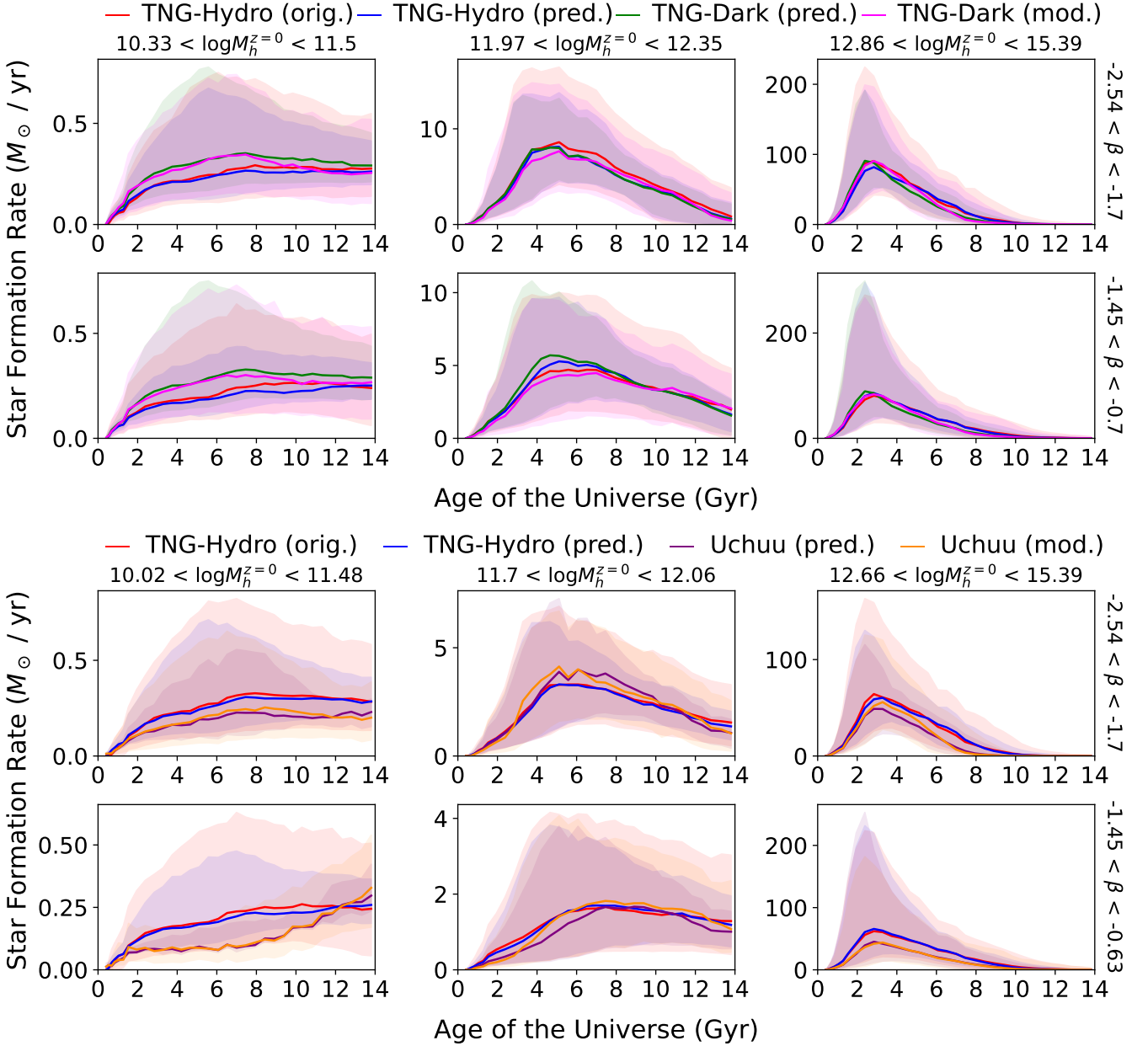


Figure 7. Star formation histories of central galaxies in bins of halo mass and specific mass accretion gradient. In low mass bins, there is an overprediction of star formation rates in TNG-Dark, and an under-prediction in Uchuu. In higher mass bins, this difference becomes smaller. The stochastic modification has shown here to reshape the shape and variance of N-body predictions to more closely resemble the original TNG data, improving upon the predictions in the hydrodynamical simulation as well. However, the modification cannot amend the poorly predicted star formation histories in low mass objects, as the predicted Fourier Transforms used by the modification are similarly affected by mass resolution.

to the average height of the relation, as well as marginally increasing the scatter. The fluctuations added by the modification add a component of stellar mass which may be attributed to events such as galactic winds or minor mergers; while the cycling of gas through the CGM acts on sub-Gyr timescales for high-mass galaxies in dense environments (Oppenheimer et al. 2010), stellar feedback is more likely to disrupt the shallow potentials of low mass galaxies and contribute to greater mass loss on short timescales (El-Badry et al. 2016; Anglés-Alcázar et al. 2017). Despite the variety of processes acting on different timescales in different mass regimes, the fluctuations implemented by the modification are rarer for the most massive

galaxies, and smaller relative to the total mass, making little change to the modified stellar mass.

At low masses, we see that the distribution of stellar masses in Uchuu is significantly biased towards low masses, owing to the compromised star formation rates. Low mass satellite haloes have already been discarded by our cuts, resulting in a clearly distinct halo mass distribution, yet there are still a large number of objects below $\sim 2 \times 10^{11} M_{\odot}$ with severely miscalculated stellar mass. Satellite objects within this mass range clearly cannot be trusted.

Low mass satellites are additionally made impractical due to a limitation of the resolution correction presented in CT23. The correction consists of a $z = 0$ halo mass dependent ratio between

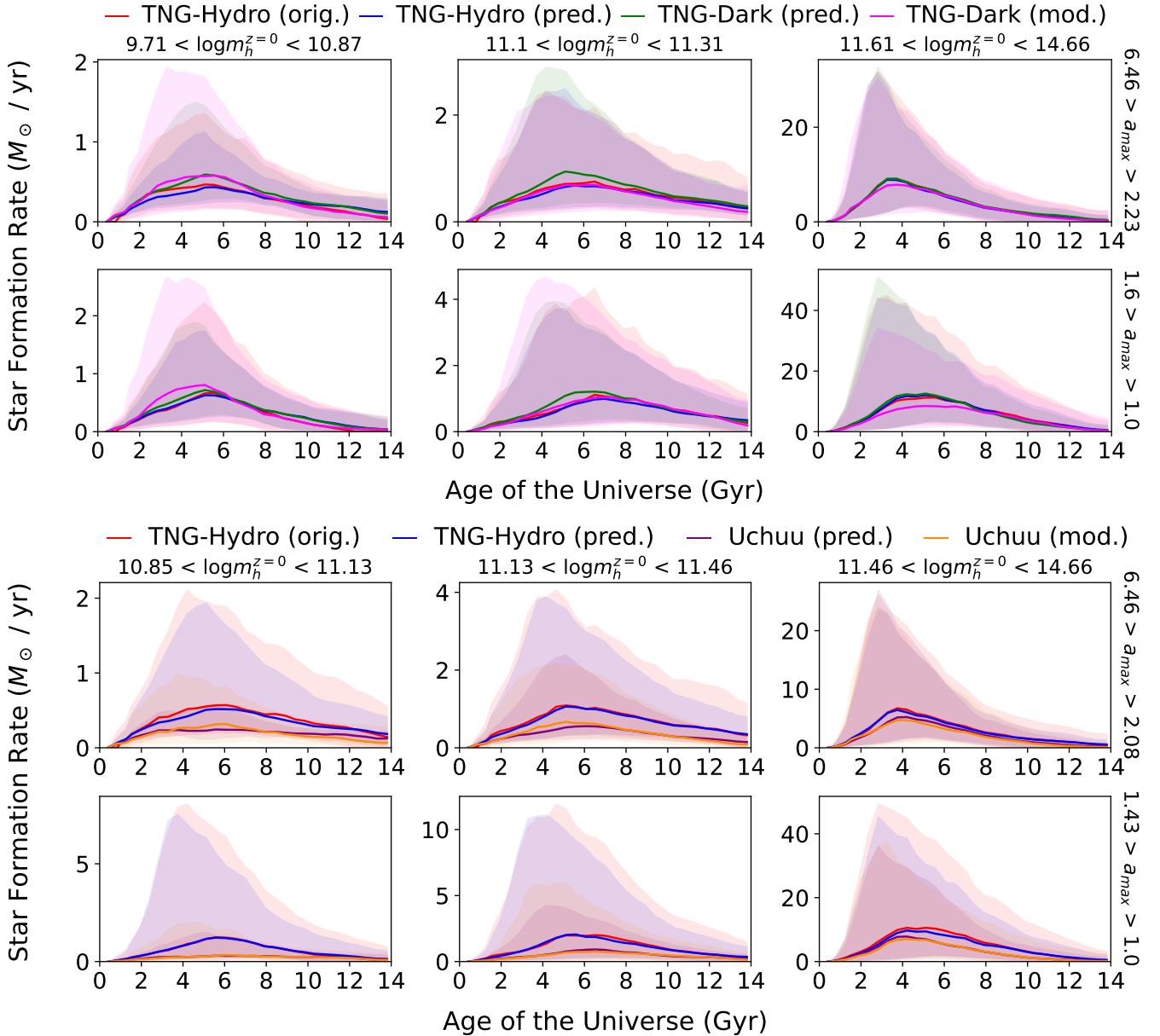


Figure 8. Star formation histories of satellite galaxies, binned in the same manner as in fig. 7. This figure shows apparently poor predictions of star formation histories of low mass galaxies in Uchuu, however many of these bins are underpopulated by the Uchuu data and contain low quality haloes.

star formation and metallicity histories in TNG100-1 and the lower resolution run TNG100-2, with a mass resolution consistent with TNG300-1; to adjust TNG300-1 galaxies to match TNG100-1 data prior to their simultaneous use as training data. For satellite galaxies, however, the correction ceases to be accurate when satellite galaxies of distinct evolutionary geometries (e.g. early-forming, quenched and late-forming, star-forming galaxies), are combined as one correction for all low mass satellites; as well as when the TNG100-2 galaxies on which the correction is based are affected by low sample size and resolution.

The correction was based on a method used by [Pillepich et al. \(2017b\)](#), who find that the radius enclosing star particles influenced their corrected data. As [Nelson et al. \(2019a\)](#) find higher gas densities in TNG300-1 than in TNG100-2, it is possible that differences in the density of gas surrounding satellites results in differences in ram pressure stripping and thus stellar mass profiles. These are two

effects which reduce the validity of the correction for satellites, particularly at low mass. It is such a substantial difference for low mass satellites that these samples are ignored when applying the stochastic correction.

In high mass bins, the majority of stellar mass is formed earlier than in TNG-Hydro, for both dark simulation suites. This is illustrated by fig. 11, which shows mass weighted ages of galaxies in bins of stellar mass, and shows that high mass galaxies are biased towards older ages. In part, this can be seen by a sharp increase in both halo and stellar mass at earlier times, but in figs. 7 and 8 the following decline in star formation rate happens sooner. The stochastic modification corrects for excess early star formation, indicating that the missing stellar feedback effect is encoded in the SFH power spectra; yet the modification does not influence the quenching tail, which is a smoother feature and so potentially unseen by the modification due to frequency-dependent phase selection, while unphysical noise

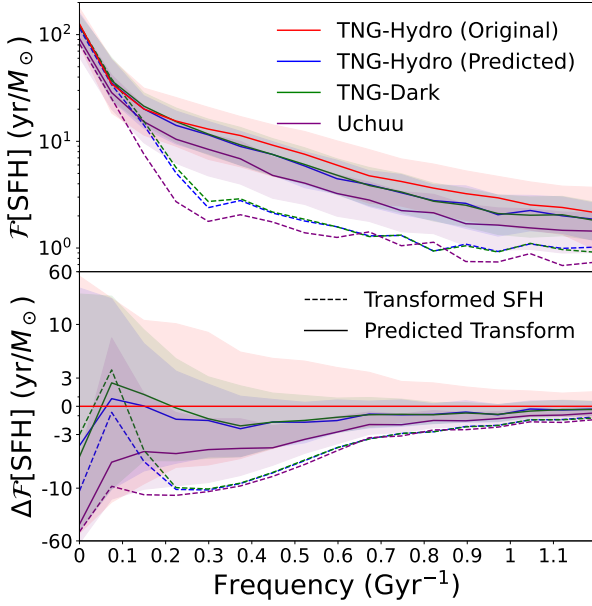


Figure 9. A figure comparing the median and interquartile ranges of predicted Fourier Transforms of star formation histories, for central galaxies where $11.97 < \log_{10} M_h^{z=0} < 12.35$ and $-1.45 < \beta < -0.7$, corresponding to the centre-bottom panel in fig. 7. The top panel of this figure shows the Fourier Transforms themselves, while the bottom panel shows the difference in the Fourier amplitude with respect to the median target amplitude. Where applicable, dashed and solid lines indicate the Fourier Transforms of the star formation histories predicted by the neural network, and the predicted Fourier Transforms when the network is trained to predict these, respectively. This illustrates that for all datasets, the median Fourier Transforms are all of similar shape to the target TNG-Hydro data (red) when predicted by the neural network. The TNG-Dark result (green) is similar enough to the TNG-Hydro predictions (blue) that the modified data in TNG-Dark will be just as accurate as in our companion paper. On the contrary, the Uchuu data (purple) has clearly suppressed amplitudes at all frequencies, and does not align with the target distribution. This suggests that star formation modes which influence our results will be absent from some of our Uchuu predictions, regardless of the power of the stochastic amendment.

in the quenching tail is eliminated by our post-processing filters (see BTC24 sec. 3.3). In Uchuu, the mass-weighted ages of intermediate mass galaxies are shifted by a lesser degree than in TNG-Dark, potentially due to differences in the accuracy of Fourier amplitudes. For TNG-Dark, star formation histories are initially aligned with TNG-Hydro, but these star formation rates decline and line up with the lower SFH in Uchuu. The quenching of these galaxies is therefore more efficient than their hydrodynamical equivalents.

Davies et al. (2019) show that the expulsion of the circumgalactic medium in TNG and the Eagle simulations (Schaye et al. 2014) is correlated strongly with the central black hole mass of the galaxy, which influence the subsequent specific star formation rate, and act on timescales of multiple gigayears (Iyer et al. 2020; Zinger et al. 2020; Walters et al. 2022). Bluck et al. (2020) show that central velocity dispersion, effectively measuring the AGN mass, is a critical parameter for galaxy quenching in MANGA observations, which correlates with the circular velocity and half-mass radius of the halo. In TNG, these internal feedback quenching mechanisms dominating central galaxy quenching, alongside environmental effects dominating satellite quenching, are shown to qualitatively agree with other hydrodynamical and semi-analytic models, and with low-redshift SDSS data (Donnari et al. 2020, 2021).

We have shown in fig. 4 that the half-mass radius of high mass

haloes is underestimated in TNG-Dark, leading to overestimated halo concentration. This velocity dispersion measures the dynamics of the halo centre on sub-kiloparsec scales, and therefore the halo concentration relates to the density of this region, which in galaxies of this mass are most likely to be dominated by an AGN. Overestimating the concentration can cause overprediction of AGN feedback, thereby quenching the galaxies sooner.

4.2 Metallicity History

Figures 12 and 13 show the median and 15th – 85th percentile ranges of predicted metallicity histories. These show a clear failure of the model to predict the metallicity histories of low mass objects in Uchuu, as well as underpredicted results in most satellite galaxies. There is nonetheless a good agreement between Uchuu and TNG with most intermediate to high mass central haloes.

The stochastic amendment introduces a significant improvement to the median and variance of metallicity histories. Like the star formation histories, it is likely that the network-predicted Fourier Transforms contain information on the frequency of chemical enrichment events on short timescales, such as merger-driven star formation. The simultaneous recovery of the variability in star formation and metallicity histories results in a more realistic metallicity distribution with respect to the fiducial network predictions, as shown in BTC24.

We see similar characteristics when comparing metallicity histories seen in TNG-Hydro, TNG-Dark and Uchuu to what we showed for star formation histories in section 4.1. The suppression of metal synthesis in low mass galaxies can be reconciled with the lack of early accretion, particularly as the gas and metal content of these objects’ progenitors play an important role in early metal synthesis. The enhanced metal synthesis in low mass TNG-Dark galaxies may also be explained by the absence of stellar feedback, where stars retain more of their mass and thus produce metals more efficiently.

In narrow mass bins, we find similar but weaker correlations between stellar metallicity and structural and density quantities. The results from CT23, however, suggest that environmental history influences chemical enrichment over time. We show in fig. 6 that calculated overdensities are marginally larger in Uchuu, which can influence metallicities by predicting an overabundance of mergers and flybys which redistribute the metals into high mass galaxies, as well as contribute to quenching. The anisotropic nature of these interactions are traced by radial skews, which we show in CT23 to have a profound effect on the metallicity history. Though these skews are not well correlated with other halo properties, being difficult to compare between simulations, the low number density of haloes around low mass objects can fail to produce the extreme skews experienced during close interactions which contribute significantly to chemical enrichment.

Evaluating the mass-metallicity relations from these star formation and metallicity histories in fig. 14, we see that the underpredicted metallicity histories distort both relations at the low mass end. Nevertheless, the shape and scatter of the relations in the dark simulation are very similar to the network’s original TNG-Hydro predictions; particularly following stochastic modification. For central galaxies, however, there are a handful of overpredicted metallicities in the dark simulations at high mass. A Spearman coefficient of 0.683 between age and metallicity for Uchuu galaxies above a stellar mass of $10^{11.5} M_{\odot}$ shows that these are the same galaxies whose mass-weighted ages are overpredicted. Therefore, there is a greater contribution of metallicity histories at early times to these results, and negligible contribution from when the galaxies begin to lose

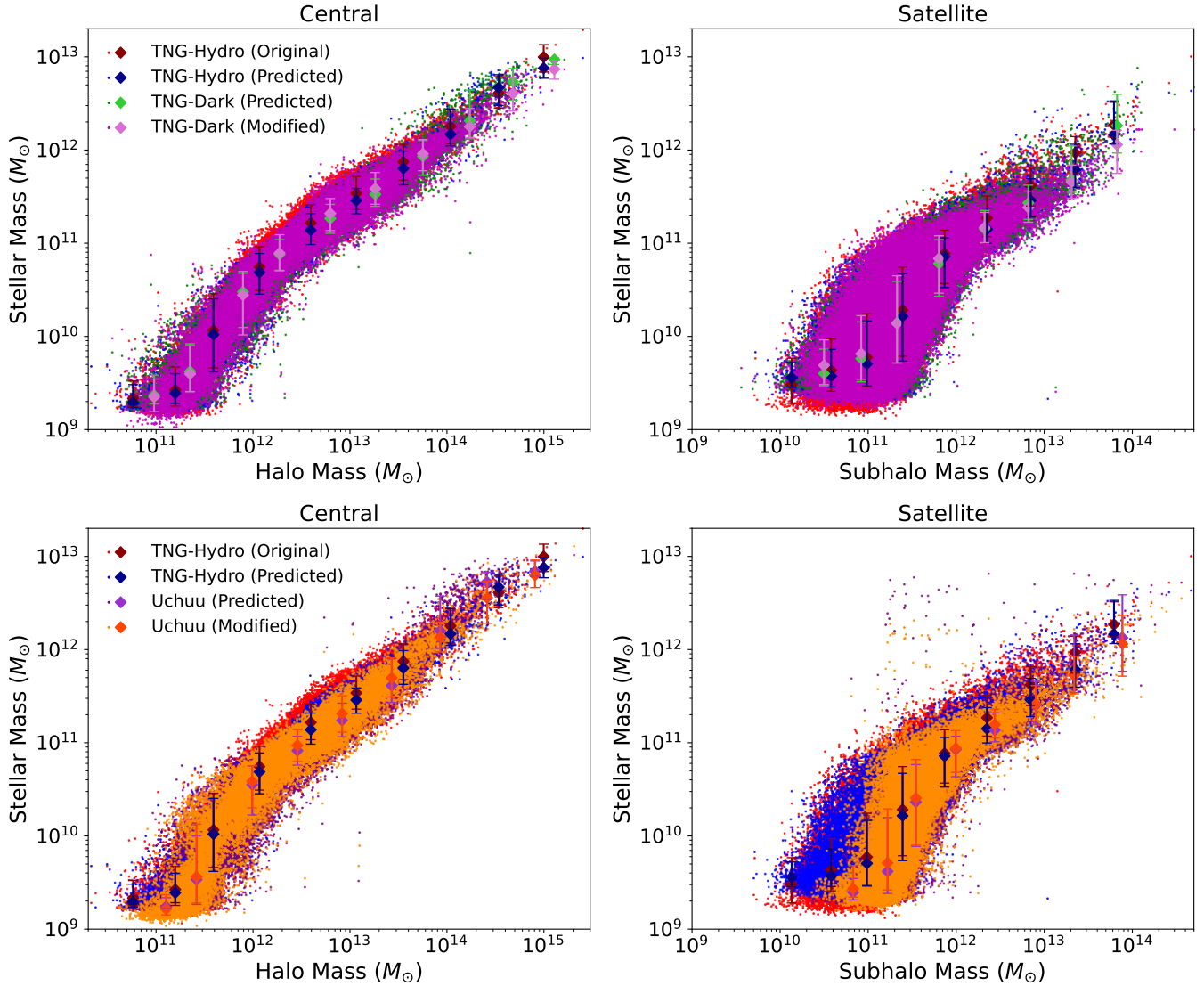


Figure 10. The graph displays the numerical SHMR of central galaxies (left) and satellite galaxies (right) based on their star formation rates. Each galaxy is represented by a data point, while the error bars indicate the median and 15th and 85th percentiles of stellar mass within a specific halo mass range. The comparable shapes of these relationships suggest an accurate prediction of the star formation histories.

their star formation. This effect is subsequently mitigated by the stochastic amendment, reducing the coefficient to 0.135; similar to the TNG-Hydro target value of 0.217. As previously established, the modification shifts the early star formation towards the TNG target; but additionally adds fluctuations which enhance the chemical evolution across all times. This improvement, not only to the stellar formation time, but to the characteristic time of metal synthesis, is of great value for refining the predicted spectroscopy which would be used in N-body mocks. We discuss these results in the following section.

5 MOCK OBSERVABLES

This section concerns how the previously described similarities and discrepancies between halo and galaxy properties affects the derived observational results, and thus is an assessment of the quality of hypothetical mock survey statistics.

5.1 Galaxy Spectra

We show in figs. 15 and 16 the spectral energy distributions of the four simulation datasets in bins of stellar mass, for central and satellite galaxies. In CT23 we relate the smaller variance of the predicted SEDs to the lack of variability in star formation histories, and unconstrained implicit features such as merger-driven starbursts and quenching timescales, which are more common to central galaxies.

The mean amplitudes of TNG-Dark spectra are subtly smaller for low and intermediate mass central galaxies, and larger for satellites. The satellite discrepancy can be attributed to higher peaks in star formation histories at such masses. While this affects both networks, the effect is particularly prominent for satellites, which in addition to the absence of stellar feedback driven mass loss (Sorini et al. 2022), may be likened to the lack of environmental harrassment serving to strip the satellite halo following infall (Engler et al. 2020), as discussed in section 4.1. For central galaxies, the cause of this offset is not clear, but given differences in star formation histories and mass-

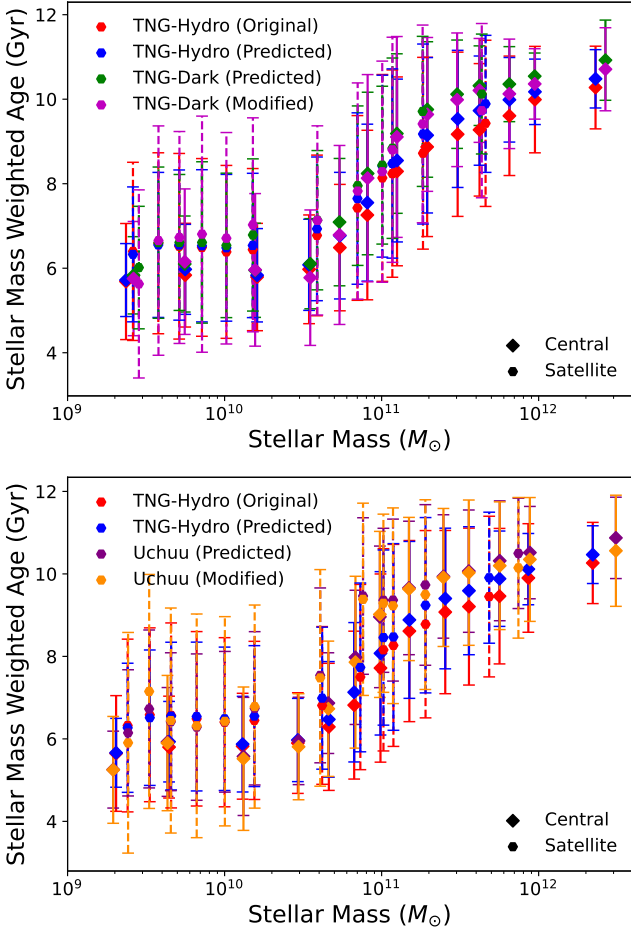


Figure 11. The figure depicts the mass-weighted ages of central and satellite galaxies, showing TNG-Dark results in the top panel and Uchuu results in the bottom panel. The ages are plotted against the predicted stellar mass, with the median and interquartile range of ages shown in various mass bins. The plot reveals a precise recovery of the age-mass trend in the dark simulations. There is a bias towards higher ages in the dark simulations which grows with mass, partially corrected by the stochastic modification.

weighted ages, the offset may owe to the underpredicted star formation histories seen in Uchuu predictions.

The stochastic modification systematically increases these galaxy luminosities as it does with stellar masses, therefore it improves the spectral amplitudes for central galaxies, and not satellites, which additionally exhibit greater variance than the target data when compared with central galaxies. While central galaxies tend to quench as a result of mergers and AGN growth, satellite quenching can be driven by the environment imposed by its host galaxy, and can act on short and on long timescales, depending on infall trajectory, satellite-host mass ratio and redshift (Baxter et al. 2022; Mao et al. 2022); potentially explaining this inconsistency between the spectral modifications of central and satellite galaxies as a matter of the physical processes which act in the effective frequency range of the stochastic modification.

In Uchuu, the spectra are generally lower in amplitude than TNG-Dark spectra, resulting from weaker star formation histories. One exception is low mass central galaxies, which may be a result of poorly predicted metallicity. In high mass bins, however, the variance in Uchuu spectra is larger than that of any TNG data, corresponding to larger variance in mass accretion histories. The large spread of

Uchuu overdensities in high mass bins will additionally have misled the network, either by enhancing star formation by associating densities with merger rates, or conversely, suppressing it by association with quenching. In fact, the Spearman coefficient between zero-redshift overdensity and each band magnitude is on average -0.43 for galaxies above $10^{11.5} M_{\odot}$, compared with -0.09 overall. The stochastic amendment may reshape these large Uchuu galaxy spectra to more closely resemble that of TNG galaxies, but of course cannot reduce the variance as needed, only reducing this average Spearman coefficient to -0.38 .

5.2 Galaxy Photometry

In fig. 17, we show the colour-mass diagrams evaluated from the four simulation datasets, showing for both central and satellite galaxies, the dependence of colours calculated using neighbouring SDSS wavebands on their stellar mass. As in CT23, these results show the bimodal colour distributions of the galaxy populations, and the tendency for high mass galaxies to be redder in colour, to be a feature of all predictions of the neural network. This work showed that the unconstrained emission at UV frequencies has resulted in underpredicted colours for u and g bands, which shows in the dark simulations as well. While the stochastic modification recovers the widths of the bimodal colour peaks, owing to improved variance in star formation and spectral amplitude, it fails to correct the offset peak in $u - g$ colour, suggesting the need to accurately predict recent star formation to accurately constrain key spectral features such as the 4000\AA break.

In the predictions of the dark simulations, there are some notable differences with respect to the predictions of the hydrodynamical simulation. The ages of high mass galaxies are biased towards high values in both dark simulations, as shown in fig. 11; and correspondingly, a higher fraction of galaxies reside in the "red" peak in these datasets, particularly for $u - g$ and $g - r$ colours. This overabundance of red galaxies is potentially a result of a greater rate of galaxy quenching, which was discussed in section 4.1 in relation to the differing morphology of haloes in dark simulations; or the denser environments in dark simulations which serve to quench interacting or infalling galaxies. The stochastic modification partially corrects this by reshaping the star formation histories, making some red galaxies bluer by eliminating excess early star formation, but does not recover quenching tails which would also shift these colours.

Another aspect of the dark predictions is the greater abundance of galaxies in the "green valley": the transition phase between star-forming and quiescent galaxies. This feature applies to both dark simulations, but is particularly prominent in Uchuu. Unlike the colour offset arising from the galaxy age bias, galaxies in this mass range typically have a broader range of calculated magnitudes, which, like the high variance in spectra, may be attributed to variations in the halo mass accretion history and internal dynamics. Furthermore, an effect of the stochastic modification is the enhancement of the green valley population; as the modification is sensitive to a frequency range which captures a specific set of star formation features, the correction it implements may only constitute a partial shift in the photometric colour.

We have shown in CT23 that the variability in star formation history, particularly at late times, is an important factor in modelling photometry. Even in cases where the Fourier Transforms of Uchuu galaxies are well predicted, the star formation histories in Uchuu may have lost additional high frequency information from being based on temporal predictors which were interpolated over a sparser time domain in Uchuu, which could not be rectified by a TNG-based

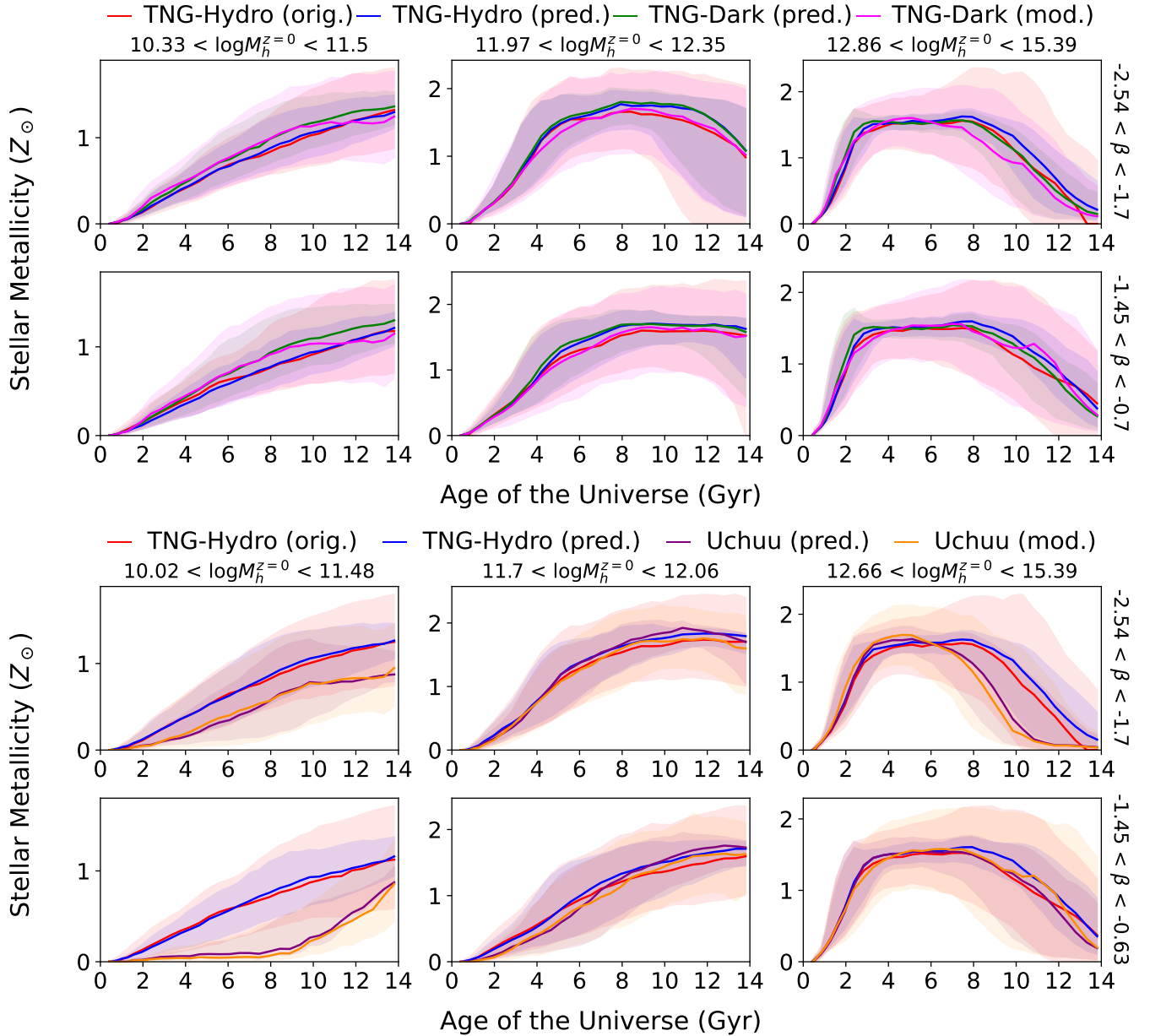


Figure 12. Stellar metallicity histories of central galaxies in bins of halo mass and specific mass accretion gradient.

stochastic modification. Uchuu galaxies in this mass range are also slightly redder on average than TNG-Dark, which corresponds to declining star formation histories in this mass range. In fact, this effect is seen at the approximate mass at which biased galaxy ages begin to appear, suggesting that over-quenching is indeed a prevalent issue. This emphasises the importance of constraining late star formation to accurately predict observable data.

This modification is additionally only able to correct for differences in network predictions which translate to intermediate frequency modes in the star formation history, including supernova feedback but not necessarily slow quenching. Concerning high mass galaxies, [Iyer et al. \(2020\)](#) show that kinetic AGN feedback introduces a variable star formation component, which in TNG contributes significant energy injection only above a threshold black hole mass of $\sim 10^8 M_\odot$; unlike the thermal feedback mode, whose energy yield is tightly correlated with this AGN mass ([Zinger et al.](#)

[2020](#)). These distinct modes of AGN feedback may explain why the stochastic modification can only partially amend the geometry of quenched star formation histories; the kinetic feedback resides in the frequency domain of the modification, while the long-timescale thermal feedback is closely related to AGN mass. While AGN mass is not predicted directly by this model, it is closely related to star formation history, and so the effects of thermal AGN feedback will be influenced by the established shortcomings of the fiducial neural network predictions, in both the hydrodynamic and the dark simulations.

6 DISCUSSION

The machine learning model used to predict the star formation and stellar metallicity histories of TNG galaxies has performed modestly at reproducing the same results in pure dark matter simula-

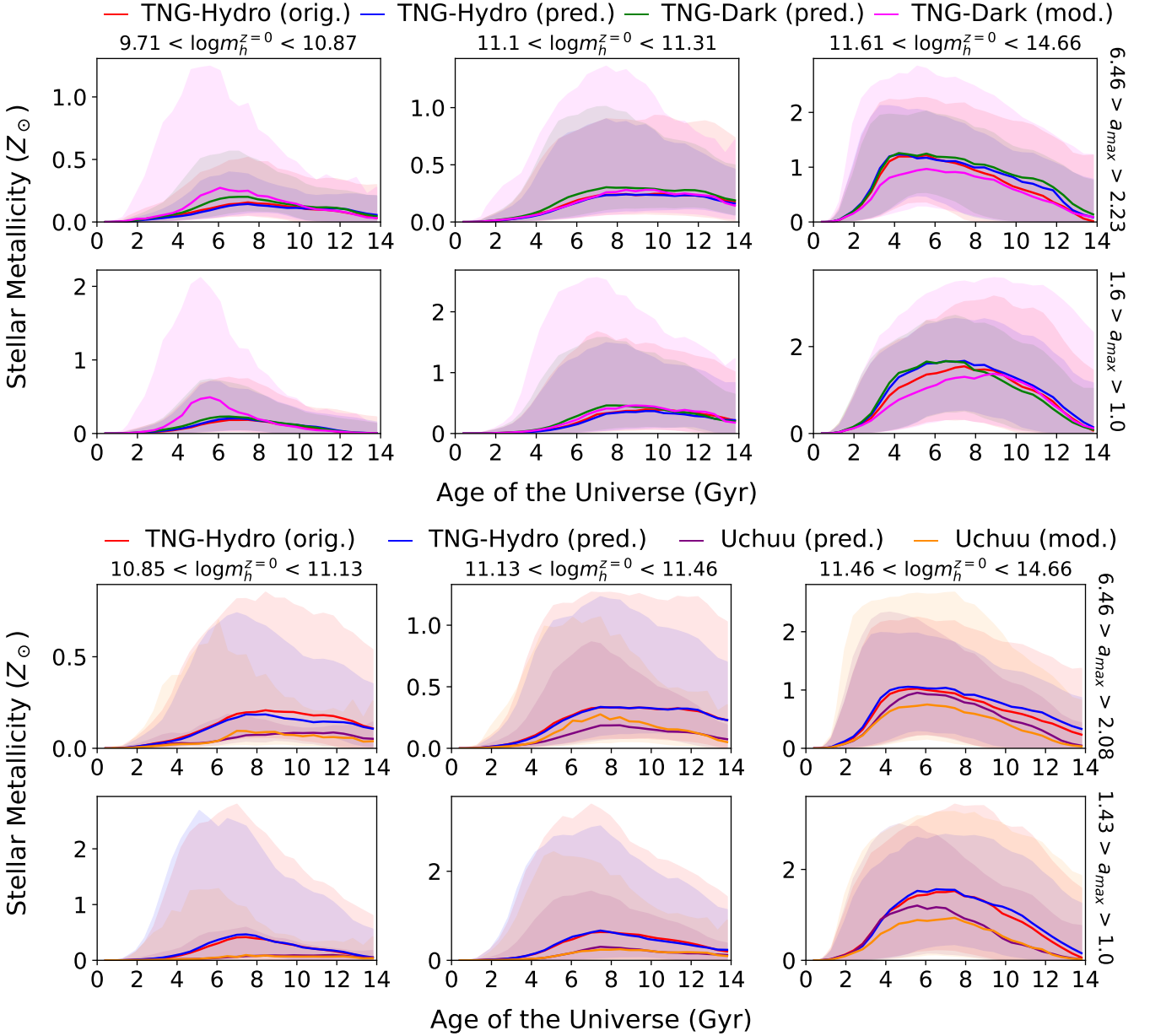


Figure 13. Metallicity histories of satellite galaxies, binned in the same manner as in fig. 12.

tions, having obtained similar quantitative relations between galaxies and haloes, and relating physical galaxy properties to observational quantities as in the hydrodynamical TNG simulation. Despite this, a number of discrepancies exist between the different predictions, resulting from differences in the growth and interactions of haloes in N-body simulations compared with the full physics, differences in the calculation of halo properties in the simulation data, and the degree of improvements made by stochastic modification. In this discussion, we identify the important differences between these simulations and how the model may be modified in future to suit high volume N-body simulations while maintaining an accurate characterisation of the galaxy-halo connection.

6.1 Resolution Effects

We have shown that the lower resolution of the Uchuu simulation compared with the TNG simulations has worsened the quality of predictions of low mass and slowly accreting galaxies, with considerable errors in the masses and metallicities of low mass galaxies; particularly satellite galaxies, whose sampling was already compromised by our quality cuts. One such effect is that the truncated power spectrum suppresses the coalescence of simulation particles into low mass haloes, such that low mass haloes take longer to germinate and grow. Low mass samples in Uchuu are evidently unreliable for causal galaxy-halo modelling. The SFH and ZH Fourier Transforms predicted by this model are poorly predicted for these haloes as well, indicating that resolution differences additionally effect our stochastic methodology.

The limits of computational resources required to generate a high-volume, high-resolution simulation has been a long-standing issue

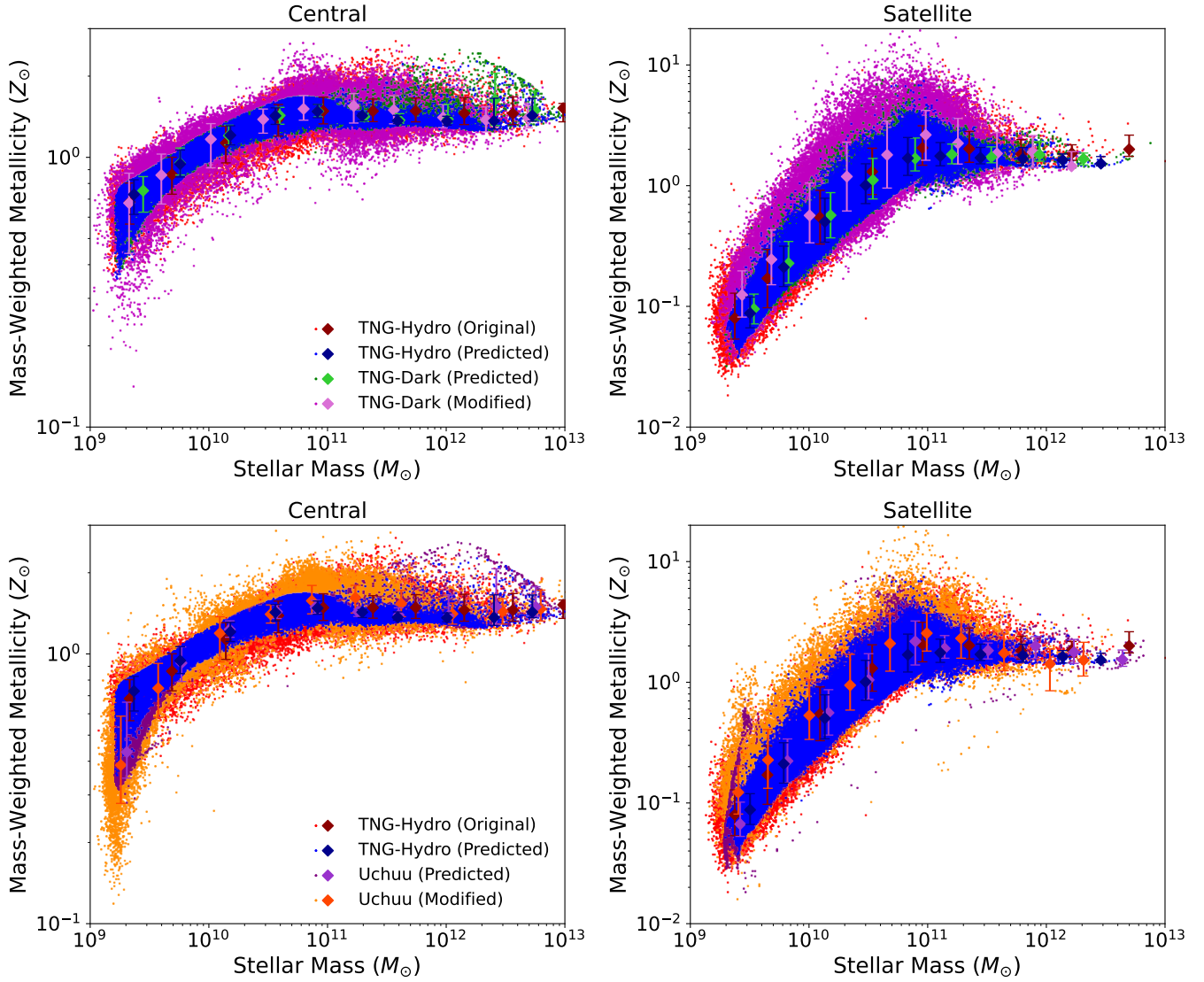


Figure 14. Numerical MZR of central galaxies (left) and satellite galaxies (right), with numerically evaluated total stellar mass and mass-weighted metallicity.

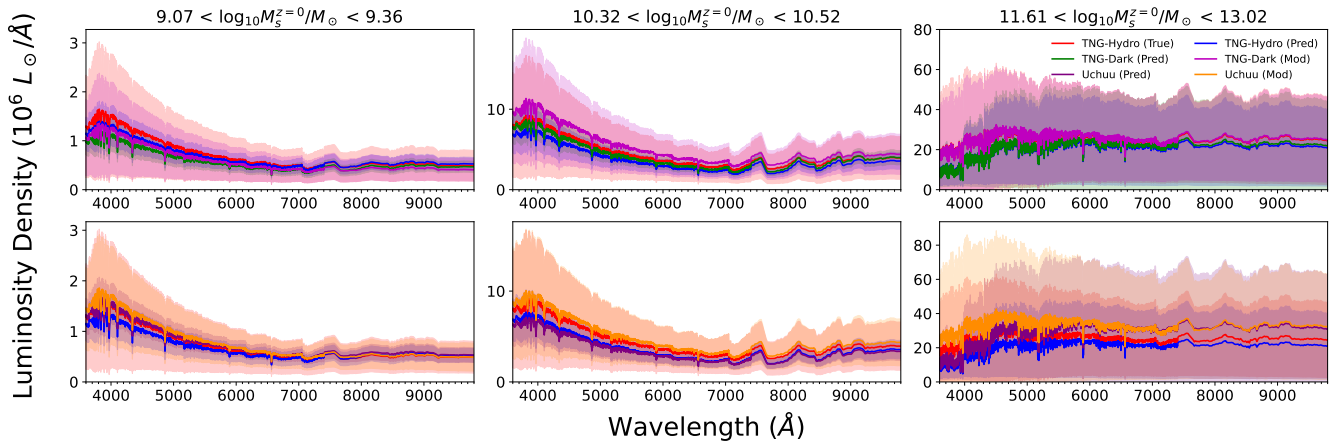


Figure 15. For central galaxies, this figure shows the evaluated SEDs in TNG-Dark (upper panels) and Uchuu (lower panels) in contrast with the TNG-Hydro data. For each dark simulation, the spectral luminosities are on average under-predicted slightly, but this is improved by the stochastic modification, which also serves to restore some of the variance in these spectra. Emission lines are not shown in these spectra, for the sake of clearly showing the mean continuum from each simulation.

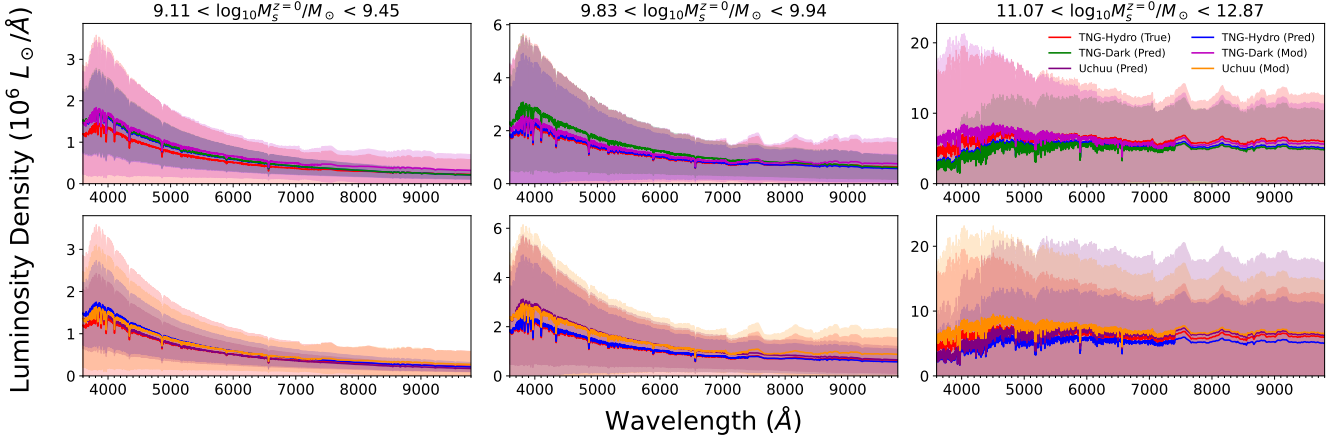


Figure 16. For satellite galaxies, this figure shows the evaluated SEDs in TNG-Dark (upper panels) and Uchuu (lower panels) in contrast with the TNG-Hydro data. The two dark simulations are well-matched to the predictions in the hydrodynamic TNG simulation, showing similar means and variances in the spectra. This causes the average luminosity to be brighter than needed following modification, but like the central galaxies, the modification recovers the variance originally seen in spectral luminosities. As with fig. 15, emission lines are omitted from the figure for clarity.

in this field. Li et al. (2021) demonstrate a machine learning model which can enhance the matter power spectrum in N-body simulations and generate accurate snapshot data from low-resolution simulation images, which accurately replicate halo substructures and correlation functions below the limit of said low-resolution simulations (Ni et al. 2021). This may be a practical technique to enhance the Uchuu data in this work, provided that the complete merger trees can be constructed from the model’s outputs. Given the importance of the properties of progenitor subhaloes, such as the mass and metallicity of incoming gas and stars, it may be necessary to develop a similar enhancement model of the merger trees themselves; however, as the matter power spectra, distributions and velocity fields can be accurately enhanced this way, these properties may be inferred from the predicted environments.

Our results show that haloes in Uchuu of similar mass to the lowest mass haloes in TNG are substantially affected by the difference in resolution, and thus, it may be worthwhile in a future study to apply the neural network to Shin-Uchuu: a smaller but higher resolution run of the Uchuu model, to restore low mass galaxies; or to enhance the Uchuu snapshots and merger trees based on the superior Shin-Uchuu resolution and the methods of Li et al. (2021). As the growth of large scale structure will influence the distribution of galaxies and the properties of their environments, the latter may be a more suitable method for creating self-consistent mock catalogues on both gigaparsec and sub-kiloparsec scales.

6.2 Alternative Models

6.2.1 Uchuu-UniverseMachine

Aung et al. (2022) use the UniverseMachine (UM) model (Behroozi et al. 2019a) to compute galaxy formation histories in the Uchuu simulation, which is used to recover statistics such as stellar mass functions and number density profiles which show reasonable agreement with observational stellar mass and luminosity functions (Behroozi et al. 2019b). UM is an empirical model, relying on MCMC optimisation of star formation rates using prior relations of star formation rates and quenched fractions to the halo rotation curve. The model was able to qualitatively reproduce the environmental dependence of star formation without explicit implementation of the environment, yet this implies that the star formation in

dense environments is only supported by halo mass accretion. UM does not model metallicity histories, which we have shown in CT23 to be more dependent on environmental quantities, and thus our model may be more suitable for modelling the dependence of chemical enrichment in high fidelity mocks. On the contrary, as quenched fractions are a direct parameter of the UM model, the colour bimodality in these mocks is likely to be more accurate, and so UM may be more suitable for observational statistics.

A predictive, self-consistent model such as ours may prove complementary to empirical models such as UM when it comes to producing high-fidelity mocks, as it can be used to causally model the growth of galaxies over time based upon the halo and environmental quantities driving the physics of the galaxy-halo connection, and may be modified to predict galaxy properties, for instance, spiral-bar structures. Yet, our machine learning model and stochastic modification have shown to be sensitive to effects which come from translation to a pure dark matter simulation, such as the biased growth of internal dynamics of the halo, resolution effects such as the delayed collapse and virialisation of haloes, and potentially, nuances in the calculation of key variables such as halo mass and radius due to the use of different halo finder algorithms; which may, for instance, identify different structures in the halo centre, or different boundaries enclosing the total halo mass (Onions et al. 2012). Thus, it may prove that an N-body simulation with resolution enhancements and consistent halo definitions with the training data will be necessary for accurate self-consistent mocks.

6.2.2 Gaussian Process Stochasticity

Our stochastic modification to the star formation and metallicity histories has proven valuable in recovering the short-timescale features which were absent from the fiducial neural network model, corresponding to relevant phenomena such as starbursts and baryon cycling. It is nonetheless difficult to disentangle the physical drivers of these stochastic features, which have different degrees of influence depending on a galaxy’s mass, age and environment. To analyse the relative contribution of these dynamical processes to observable features such as the H- α flux and D_n4000 index, one might incorporate a Gaussian process formalism as seen in Iyer et al. (2024), where the stochastic modes of star formation are parameterised by three analytic power spectra with controlled effective timescales.

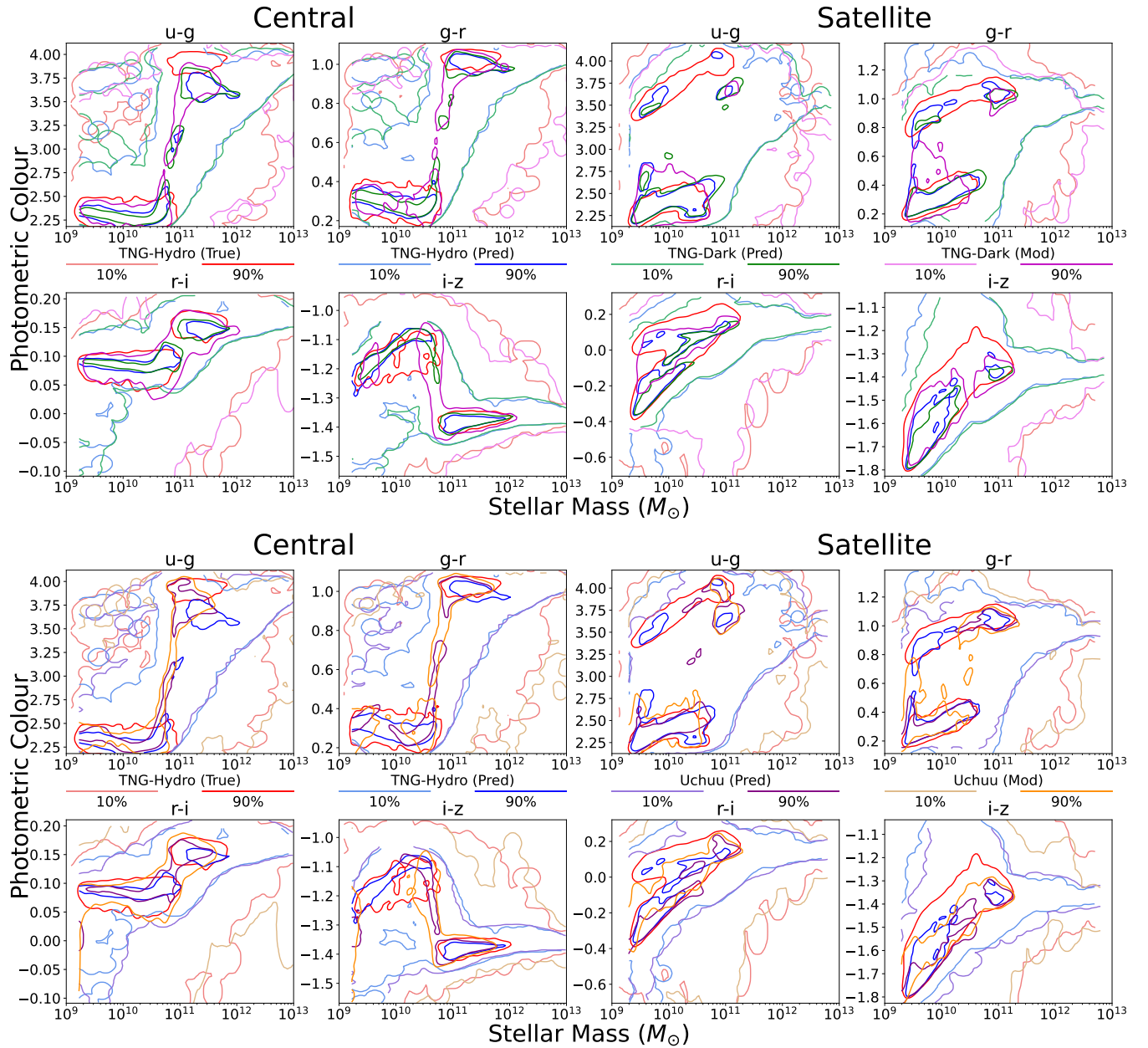


Figure 17. Colour-Mass diagrams from each of the four simulation datasets, shown for central galaxies (left panels) and satellite galaxies (right panels), and for four colours taken as the difference between successive SDSS band magnitudes. Contour lines show the 10th percentiles (light-coloured lines) and the 90th percentiles (dark-coloured lines) of the 2D histograms of the data. The predicted photometric colour bimodality and its association with mass are shown by all datasets, however the dark simulations show an excess of samples in between the peaks of the colour distributions. The stochastic modification redistributes the colour distributions, recovering the full range of colours seen in the original data, but does not rectify the offset peaks of the distribution, particularly for high friends.

Our stochastic phase selection method presented in [BTC24](#) considers the cross-correlation of modes of halo and galaxy growth, and so the evolution of the host halo may provide some insight into constraining these timescales for individual galaxies, if these two stochastic analyses can be reconciled. This may require more historical information than what was presented in our companion paper, considering that the gas inflow and cycling studied by [Iyer et al. \(2024\)](#) are potentially sensitive to environments; but if the stochastic parameters can be inferred solely from properties of the halo and environment, they can contribute to self-consistent predictions in N-body simulations.

6.3 Alternative Variables

The variables used in the design of our neural network were meant to characterise the growth, structure and environment of haloes in a manner which was as immune to the effects of baryons and different resolutions and halo finders as possible. However, the results have shown that these differences have nonetheless produced small to substantial differences in the statistics of galaxies predicted using pure dark matter simulations with respect to the hydrodynamical TNG model. Thus, the inclusion of as-yet unused variables in a future rendition of the neural network model may constitute more suit-

able measures of the galaxy-halo connection for use in a pure dark matter model.

As mentioned in section 6.2, the use of a consistent halo finder in the hydrodynamical and N-body simulations under consideration may be necessary to avoid biasing predictions due to the different identification of halo mass and substructure. Onions et al. (2012) state that while many halo finder algorithms are alike in their capability of identifying halo structures, Rockstar is the only algorithm in this study which accurately resolves substructures in highly dense regions such as the halo centre, which can influence the structural variables $R_{\frac{1}{2}}$ and \tilde{v}_{vir} ; shown in CT23 to influence the SHMRs of both central and satellite galaxies. The planned TNG halo catalogue based on the Rockstar halo finder may be used to train an "Uchuu-friendly" neural network model in future research, effectively eliminating this potentially appreciable biasing factor.

Another quantity which differs between the simulations in this study is overdensity, which in Uchuu is computed using halo coordinates and masses in lieu of similar subhalo information as in TNG. Overdensities may be smoothed according to a Gaussian kernel to produce a continuous, position-dependent density field as in Chen et al. (2020), which may be tuned for each simulation according to their resolution or their density tracers. This method was used similarly to create a position-dependent tidal field tensor, which the authors show to correlate strongly with halo assembly bias.

For satellite galaxies, the environment they experience in the vicinity of their host halo dominates their behaviour in the satellite phase, and therefore the properties of the host are additionally important. In CT23 we mention how the explicit inclusion of further satellite host properties may have been beneficial to the model; examples include formation time (Artale et al. 2018), distance from the halo centre (Engler et al. 2020; Montero-Dorta et al. 2022) and angular momentum (Bose et al. 2019). The location of the satellite with respect to the host, or of a central halo with respect to a local cluster, would constitute a tracer of the local environment, and thus could be a valuable measure of effects such as gas stripping and tidal disruption.

As the skew parameter, being mass-independent and calculated using halo positions, does not differ substantially between any of the simulations used in this work, a purely position or velocity dependent environmental metric may be a feasible solution to the bias introduced by basing environments on overdensities. However, as the skew is a measure of halo-halo interactions over time, something not characterised by smooth fields, it remains a valuable parameter of this model. Yet as mentioned in section 4.2, an effectively random error may be introduced due to the lack of low-mass objects in a low resolution simulation, which would be particularly detrimental to the major interactions inferred from high or low skews.

As for the stochastic modification, while we use stellar mass to bin samples and recover separate phase distributions, we have tested the modification with an additional halo mass binning, though this introduced errors in cases of low sample size, such as with the most massive haloes. It should be stressed here that the stochastic modification does not perfectly reconstruct important summary statistics such as the MZR, and sampling phases with respect to environment may improve this result, provided that these are well sampled. Otherwise, combining results from simulations on different scales, such as TNG50 (Nelson et al. 2019b; Pillepich et al. 2019) for small scales and MillenniumTNG (Bose et al. 2023; Hernández-Aguayo et al. 2023; Pakmor et al. 2023) for large scales, may provide enough data to justify multidimensional phase selection.

7 CONCLUSIONS

In this work, we have compared the quality of predictions of galaxy star formation and metallicity histories in pure dark matter simulations, based on the semi-recurrent neural network described in Chittenden & Tojeiro (2023), and the stochastic star formation modelling of Behera, Tojeiro & Chittenden (2024). We have compared our original predictions with cross-matched haloes from the dark equivalents of the TNG simulations on which the model was trained, evaluating the effects on predictions due to the absence of baryonic processes; and we have applied the model to similar haloes from the Uchuu N-body simulation, to evaluate the effects of alternative halo definitions, and the lower mass resolution of the simulation.

Our findings can be summarised as follows:

- Important input properties such as the mass accretion history of a halo are similar between the simulations under consideration, for haloes of most masses and mass accretion gradients, as defined in Montero-Dorta et al. (2021) and Shi et al. (2020). Nevertheless, we show in section 3.1 that the mass accretion histories of TNG-Dark haloes are exaggerated, potentially as a result of the lack of stellar feedback shaping the haloes. This has noticeable, similar influence on the star formation histories of low mass galaxies, as shown in section 4.1. As this difference in mass accretion histories arises at early times, the consequential effect on the star formation histories applies for most of the time domain of the simulation, due to the recurrent design of the neural network.

- The network quantities relating to internal structure and dynamics: the half-mass radius and virial velocity of the halo, are similarly affected by the lack of baryons, but are more profoundly affected by the lower resolution of the Uchuu simulation, which becomes apparent in section 3.2. This causes the germination and initial growth of haloes to be delayed and for the mass accretion and concentration of Uchuu haloes to appear smaller than their TNG equivalents. For low mass and slowly growing haloes, these effects are dramatic, due to the sensitivity of these results to the simulation resolution.

- We show largely similar neural network predictions to the original, hydrodynamical predictions in section 4, which recover similar shape and scatter to the hydrodynamical SHMR and MZR. Despite this success, the severely underpredicted growth of low mass haloes in Uchuu leads to poor predictions of the star formation and metallicity histories of low mass galaxies. Conversely, TNG-Dark results are overpredicted due to excess mass accretion at early times, which leads to an effective overabundance of star-forming gas. In each case, the lowest mass galaxies in any dark matter simulation are the least accurate predictions.

- With the added stochastic modification, we make significant improvements to key statistics of the dark simulations, recovering the scatter of the mass-metallicity relation and correcting the spectral luminosity and photometric colour distributions of predicted galaxies. While this amendment is shown to fruitfully reproduce the missing features in the hydrodynamic TNG simulations in our companion paper, it also rectifies systematic distortions in the geometry of the star formation and metallicity histories in these pure dark matter simulations, providing more accurate predictions for future N-body mocks. However, it does not amend the issues which largely apply to low mass, under-resolved objects, where the predicted Fourier Transforms are under-predicted, thereby failing to provide adequate information to compute realistic baryonic data. The modified data is therefore just as sensitive to resolution effects as the fiducial predictions.

- In both dark simulations, the number of quenched galaxies pre-

dicted by the neural network is larger than the hydrodynamical result. In TNG-Dark, this is a result of the difference in structural parameters, which may be attributed to AGN feedback. In Uchuu, this is an effect of higher overdensities, which owe to the use of halo tracers rather than subhaloes. This excess quenching corresponds to a greater abundance of photometrically red galaxies, which we show in section 5. In Uchuu, the abundance of red galaxies is further attributed to underpredicted Fourier amplitudes, and possibly interpolation over a coarser time domain, resulting in greater information loss regarding time variations in their star formation history. The stochastic modification serves to redistribute the photometric colours by reshaping the star formation histories, but does not amend differences in the shapes of quenching tails, leading to some "partly corrected" photometry, and an overabundance of green valley galaxies. The spectroscopic and photometric statistics of the dark matter simulations nonetheless show similar characteristics to the original TNG results, yet this could be improved by explicit constraints on star formation at the lowest redshifts.

This paper has shown that the neural network model we have developed is a highly practical tool for emulating galaxies into N-body simulations using the learned physics of the galaxy-halo connection. However, the shortcomings of the study illustrate the necessity for an N-body simulation of similar mass resolution and halo properties to compute accurate mock surveys on all mass scales. This may be achieved in future work by redesigning the predictive model to measure halo structure and cosmic environment using identical halo finders, metrics which are independent of the simulation, or by enhancement of existing low-resolution haloes and merger trees using machine learning or similar methods.

By obtaining results in the Uchuu simulation with similar characteristics to the TNG simulation suite on which the model was trained, we have shown that it is possible to produce a physical, self-consistent model of the galaxy-halo connection on present-day, gigaparsec-scale N-body simulations. This may be a pathway to a future of AI-based simulations which entail a physical explanation of galaxy evolution on cosmological and substructure levels simultaneously, and corresponding observational data to complement the most ambitious galaxy surveys to date, for a fraction of the computational cost of a hydrodynamical or semi-analytic model of the same level of detail.

ACKNOWLEDGEMENTS

The UKRI Science and Technology Facilities Council supported this study under grant ID ST/T506448/1, which the authors gratefully acknowledge. We appreciate the IllustrisTNG project allowing us access to their data and JupyterLab environment, and the Uchuu and YTree projects for access to Uchuu halo merger trees. We also thank Katarina Kraljic for assistance with modelling the cosmic web in Uchuu, and we thank Daniele Sorini and Kartheik Iyer for useful discussion on the role of gas-rich progenitors on developing halo shapes, and the influence of different modes of baryon cycling and AGN feedback in galaxy evolution models, respectively.

DATA AVAILABILITY

The principal author is currently willing to provide the information that backs up the research's conclusions upon reasonable request. The data will later be posted online for general access.

REFERENCES

- Anbajagane D., Evrard A. E., Farahi A., 2021, *MNRAS*, 509, 3441
 Anglés-Alcázar D., Faucher-Giguère C.-A., Kereš D., Hopkins P. F., Quataert E., Murray N., 2017, *MNRAS*, 470, 4698
 Artale M. C., Zehavi I., Contreras S., Norberg P., 2018, *MNRAS*, 480, 3978
 Aung H., et al., 2022, *MNRAS*, 519, 1648
 Baxter D. C., et al., 2022, *MNRAS*, 515, 5479
 Behera J., Tojeiro R., Chittenden H. G., 2024, *MNRAS*
 Behroozi P. S., Wechsler R. H., Wu H.-Y., 2012a, *ApJ*, 762, 109
 Behroozi P. S., Wechsler R. H., Wu H.-Y., Busha M. T., Klypin A. A., Primack J. R., 2012b, *ApJ*, 763, 18
 Behroozi P., Wechsler R. H., Hearin A. P., Conroy C., 2019a, *MNRAS*, 488, 3143
 Behroozi P., Wechsler R. H., Hearin A. P., Conroy C., 2019b, *MNRAS*, 488, 3143
 Bluck A., et al., 2020, *MNRAS*, 499, 230
 Bose S., Eisenstein D. J., Hernquist L., Pillepich A., Nelson D., Marinacci F., Springel V., Vogelsberger M., 2019, *MNRAS*, 490, 5693
 Bose S., et al., 2023, *MNRAS*, 524, 2579
 Castro T., Borgani S., Dolag K., Marra V., Quartin M., Saro A., Sefusatti E., 2020, *MNRAS*, 500, 2316
 Chalela M., Sillero E., Pereyra L., Alejandro García M., Cabral J. B., Lares M., Merchán M., 2021, *Astronomy & Computing*, 34, 100443
 Chen Y., Mo H. J., Li C., Wang H., Yang X., Zhang Y., Wang K., 2020, *ApJ*, 899, 81
 Chittenden H. G., Tojeiro R., 2023, *MNRAS*, 518, 5670
 Chua K. T. E., Pillepich A., Vogelsberger M., Hernquist L., 2019, *MNRAS*, 484, 476
 Chua K. T. E., Vogelsberger M., Pillepich A., Hernquist L., 2022, *MNRAS*, 515, 2681
 Conroy C., Gunn J. E., 2010, *ApJ*, 712, 833
 Conroy C., Gunn J., White M., 2009, *ApJ*, 699, 486
 Davies J. J., Crain R. A., Oppenheimer B. D., Schaye J., 2019, *MNRAS*, 491, 4462
 Donnari M., et al., 2020, *MNRAS*, 500, 4004
 Donnari M., Pillepich A., Nelson D., Marinacci F., Vogelsberger M., Hernquist L., 2021, *MNRAS*, 506, 4760
 El-Badry K., Wetzel A., Geha M., Hopkins P. F., Kereš D., Chan T. K., Faucher-Giguère C.-A., 2016, *ApJ*, 820, 131
 Engler C., et al., 2020, *MNRAS*, 500, 3957
 Habouzit M., et al., 2022, *MNRAS*, 511, 3751
 Haggard R., Pearce F. R., Gray M. E., Knebe A., Yepes G., 2021, *MNRAS*, 502, 1191
 Hernández-Aguayo C., et al., 2023, *MNRAS*, 524, 2556
 Hoffmann K., et al., 2014, *MNRAS*, 442, 1197
 Ishiyama T., et al., 2021, *MNRAS*, 506, 4210
 Iyer K. G., et al., 2020, *MNRAS*, 498, 430
 Iyer K. G., Speagle J. S., Caplar N., Forbes J. C., Gawiser E., Leja J., Tacchella S., 2024, *ApJ*, 961, 53
 Kurinchi-Vendhan S., Farcy M., Hirschmann M., Valentino F., 2024, *MNRAS*
 Li Y., Ni Y., Croft R. A. C., Matteo T. D., Bird S., Feng Y., 2021, *PNAS*, 118
 Mansfield P., Avestruz C., 2021, *MNRAS*, 500, 3309
 Mao Z., Kodama T., Pérez-Martínez J. M., Suzuki T. L., Yamamoto N., Adachi K., 2022, *A&A*, 666, A141
 Marinacci F., et al., 2018, *MNRAS*, 480, 5113
 Montero-Dorta A. D., Chaves-Montero J., Artale M. C., Favole G., 2021, *MNRAS*, 508, 940
 Montero-Dorta A. D., Rodríguez F., Artale M. C., Smith R., Chaves-Montero J., 2022, *e-print arXiv: 2212.12090*
 Naiman J. P., et al., 2018, *MNRAS*, 477, 1206
 Navarro J. F., Frenk C. S., White S. D. M., 1996, *ApJ*, 462, 563
 Nelson D., et al., 2015, *Astronomy and Computing*, 13, 12
 Nelson D., et al., 2017, *MNRAS*, 475, 624
 Nelson D., et al., 2019a, *CompAC*, 6, 2
 Nelson D., et al., 2019b, *MNRAS*, 490, 3234
 Ni Y., Li Y., Lachance P., Croft R. A. C., Matteo T. D., Bird S., Feng Y.,

- 2021, [MNRAS](#), 507, 1021
- Onions J., et al., 2012, [MNRAS](#), 423, 1200
- Oppenheimer B. D., Davé R., Kereš D., Fardal M., Katz N., Kollmeier J. A., Weinberg D. H., 2010, [MNRAS](#), 406, 2325
- Pakmor R., et al., 2023, [MNRAS](#), 524, 2539
- Pillepich A., et al., 2017a, [MNRAS](#), 473, 4077
- Pillepich A., et al., 2017b, [MNRAS](#), 475, 648
- Pillepich A., et al., 2019, [MNRAS](#), 490, 3196
- Planck Collaboration 2016, [A&A](#), 594, A13
- Prada F., Klypin A. A., Cuesta A. J., Betancort-Rijo J. E., Primack J., 2012, [MNRAS](#), 423, 3018
- Riggs S. D., Loveday J., Thomas P. A., Pillepich A., Nelson D., Holwerda B. W., 2022, [MNRAS](#), 514, 4676
- Rodriguez-Gomez V., et al., 2015, [MNRAS](#), 449, 49
- Schaye J., et al., 2014, [MNRAS](#), 446, 521
- Shi J., et al., 2020, [ApJ](#), 893, 139
- Somerville R. S., Davé R., 2015, [ARA&A](#), 53, 51
- Sorini D., Davé R., Cui W., Appleby S., 2022, [MNRAS](#), 516, 883
- Sousbie T., 2011, [MNRAS](#), 414, 350
- Springel V., White S. D. M., Tormen G., Kauffmann G., 2001, [MNRAS](#), 328, 726
- Springel V., et al., 2017, [MNRAS](#), 475, 676
- Tanaka M., et al., 2023, [ApJ](#), 970, 59
- Vogelsberger M., Marinacci F., Torrey P., Puchwein E., 2020, [Nat. Rev. Phys.](#), 2, 42
- Walters D., Woo J., Ellison S. L., 2022, [MNRAS](#), 511, 6126
- Wechsler R. H., Tinker J. L., 2018, [ARA&A](#), 56, 435
- Zhao D. H., Jing Y. P., Mo H. J., Börner G., 2009, [ApJ](#), 707, 354
- Zinger E., et al., 2020, [MNRAS](#), 499, 768

This paper has been typeset from a $\text{\TeX}/\text{\LaTeX}$ file prepared by the author.